ENGINEERING THE MARTENSITIC TRANSFORMATION HYSTERESIS OF NI-RICH NITI ALLOYS

A Thesis

by

BRIAN EELAN FRANCO

Submitted to the Office of Graduate and Professional Studies of
Texas A&M University
in partial fulfillment of the requirements for the degree of

MASTER OF SCIENCE

Chair of Committee,	Ibrahim Karaman
Committee Members,	Miladin Radovic
	James Boyd
Head of Department,	Andreas Polycarpou

December 2014

Major Subject: Mechanical Engineering

ABSTRACT

The shape memory behavior in NiTi alloys can be exploited for a wide variety of applications that require active materials. The application dictates the transformation temperatures and hysteresis of the alloy. NiTi alloys with high Ni contents can be precipitation heat treated to produce large changes in the transformation temperatures, as well as increases in strength and dimensional stability. The effect of aging on the M_s temperature has been previously studied in the literature; however, few studies have investigated long duration aging, and little attention has been paid to the effect of precipitate formation on the thermal hysteresis.

In the current work, a systematic study of heat treatments was performed to study the effect of aging time, aging temperature, and initial Ni composition on the transformation temperatures and the thermal hysteresis under zero stress conditions using differential scanning calorimetry. Heat treatments and NiTi compositions were chosen in order to ensure that only Ni_4Ti_3 type precipitates formed during the aging process.

The results showed aging led to three different transformation paths; single step B2-B19`, B2-R-B19`, and multiple step transformation. At low aging temperatures, the transformation temperatures were initially suppressed but increased after sufficient aging durations. At higher aging temperatures the transformation temperatures only increased with aging time. In high Ni content materials the transformation temperatures were suppressed more than in the low Ni content materials.

The thermal hysteresis was highest in materials aged at short times at low temperatures, when the average spacing between adjacent precipitates was small. As the materials continued to aged, the thermal hysteresis decreased with time. As the aging temperature increased, the thermal hysteresis decreased.

DEDICATION

For my parents, my grandmother, my brothers, my sisters, and my friends.

ACKNOWLEDGEMENTS

I am first of all grateful to Dr. Karaman, for all of the advice and support he has given me over the years. During those times when I felt that I would be unable to continue, Dr. Karaman did not let me quit on myself.

To all of my labmates I would like to express my appreciation for making the MESAM lab such a supportive and enjoyable place to work. Much of what I learned during the course of my thesis came from our discussions together. Thanks to Ebubekir Dogan, Alper Evirgen, Ankush Kolkathar, James Monroe, Ruixhan Zui, Ceylan Heyrattin, Nick Bruno, Nick Barta, Taymaz Jo, Matthew Vaughan, Liangfa Hu, and Hande Ozcan.

I would like to thank my two mentors, who took the time to train me in the lab and to teach me about shape memory; Dr. Ji Ma and Dr. Kadri Atli.

Finally, I would like to thank my family for their support and love. Thank you to my father, Ed Franco; my mother, Mita Franco; my brothers Ben and Byron; my sisters Lara and Leilani; and my grandmother, Theresa.

NOMENCLATURE

A_f	R-Austenite reverse transformation finish
DSC	Differential scanning calorimetry
FCT	Body Centered Tetragonal
FCC	Face Centered Cubic
M_s	Martensitic start transformation temperature
R_{sr}	B19'-R reverse transformation start
SMA	Shape Memory Alloy
TWSMA	Two Way Shape Memory Alloy
TWSME	Two Way Shape Memory Effect

TABLE OF CONTENTS

Page

LIST OF FIGURES

Page

LIST OF TABLES

Page

1. INTRODUCTION

1.1. Background

Shape memory alloys (SMAs) have a set of unusual properties that make them useful as both structural and functional engineering materials. For example, a pseudoelastic SMA can be strained far beyond the elastic limit of conventional metal alloys without any permanent deformation. In SMAs exhibiting the one-way shape memory effect (SME), a deformation imposed at low temperature will reverse itself upon sufficient heating. On the other hand, two-way shape memory effect (TWSME) materials are capable of transforming between two different shapes through the application of heating and cooling. These functional properties allow SMAs to be employed in a wide variety of applications; pseudoelastic SMAs are used in eyeglass frames, orthodontic wires, and medical guide wires. One-way SMAs are used to manufacture coupling devices, fasteners, and medical stents, while TWSMAs are mostly used in actuator and temperature control devices.

The SME has been studied for nearly a century since the observation of "rubberlike" behavior in Au-Cd in 1932 [1]. Since then, many alloy systems exhibiting shape memory behavior have been discovered and studied, such as NiTi (trade name Nitinol), Cu based alloys, and Fe based alloys. NiTi alloys have attracted the most attention due to their superior physical and shape memory properties. NiTi has high ductility, corrosion resistance, and good biocompatibility [2]. All three shape memory behaviors can be observed in the NiTi system [2-4].

1.2. The martensitic transformation

Shape memory behavior occurs as a consequence of the martensitic transformation, which can be observed in crystalline materials. This transformation is a solid-to-solid phase change from the austenite parent phase to the martensite phase; it can be triggered by stress, temperature, or by application of a magnetic field [3]. It occurs without diffusion; rather, the atoms shift their positions in the lattice in a shear-like, coordinated fashion. The resulting martensite has exactly the same composition as the austenitic parent phase, but a different crystal structure [4]. The transformation from austenite to martensite is known as the forward transformation, while the transformation from martensite to austenite is called the reverse transformation.

1.2.1. Thermodynamic aspects of the martensitic transformation

The martensitic transformation occurs via nucleation and growth of martensite inside of the austenite matrix. The condition for nucleation of martensite is described by:

$$-\Delta G_{ch}^{A-M} + \Delta G_{rev}^{A-M} + \Delta G_{ir}^{A-M} = 0 \quad (1)$$

where ΔG_{ch}^{A-M} is the chemical free energy change during the forward reaction, ΔG_{rev}^{A-M} is the reversible energy stored in the system, and ΔG_{ir}^{A-M} is the irrecoverable energy dissipated from the system [5]. Figure 1.1 shows the relationship of the chemical Gibbs free energies to temperature. In an ideal case, neglecting the non-chemical terms in (1), the free energies of martensite and austenite are equal at T_0, and transformation would occur at this temperature for both the forward and reverse transformations [5, 6].

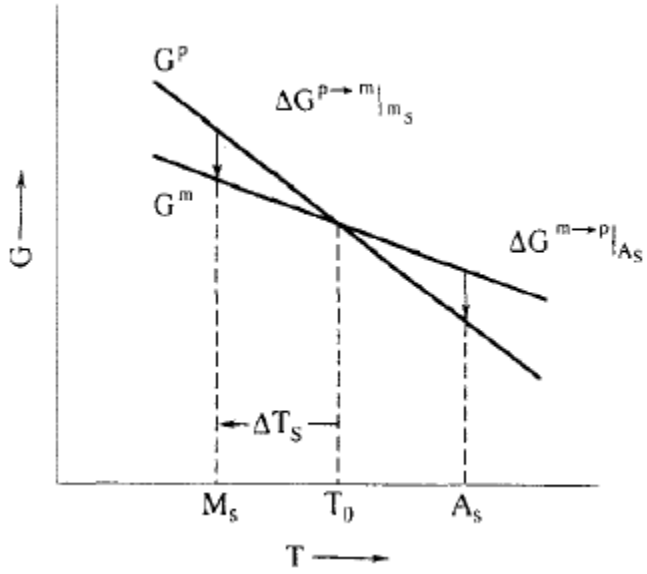

Figure 1.1 Schematic Gibbs free energy curves for an SMA showing chemical Gibbs free energy-temperature relationship [3].

However, in the case where the non-chemical elastic energy storage and irrecoverable energy terms are considered, an additional undercooling ΔT_s is required for transformation to occur. The martensitic start temperature, M_s, is the temperature at which there is sufficient driving force ΔG_{ch}^{A-M} to overcome the elastic and dissipation nucleation energy barrier during the forward transformation [7]. Further cooling below M_s will provide the necessary driving force for martensite nuclei to grow, until the transformation has been fully completed at the martensitic finish temperature M_f [8]. The nucleation and growth behavior of a martensite plate with a thickness c and radius r can be described by two steps; first, the nucleus forms at the M_s temperature and immediately grows in the radial direction until stopped by some grain boundary, free

surface, or another martensite interface. The strain energy density of the martensite nucleus is proportional to the ratio c/r. Thus, expansion of the nucleus in the radial direction reduces the strain energy density and is thermodynamically favorable [9]. Secondly, as the temperature continues to drop below M_s the martensite plates thicken in the transverse direction until an equilibrium between the chemical and non-chemical energies is reached at the martensitic finish temperature M_f [10]. During heating, at the austenitic start temperature A_s this equilibrium state is destroyed and the martensite plate begins to shrink. At A_f, the martensite completely reverts to austenite [7].

The dissipated energy ΔG_{ir}^{A-M} during transformation is attributed to two main sources, these are frictional resistance to the movement of martensite interfaces [5, 11] and the generation of defects such as twins and slip dislocations [5, 7]. The width of the thermal hysteresis is dependent on the amount of energy dissipated during the initial nucleation of the martensite interface, while the temperature difference between M_s and M_f is dependent on the reversible energy stored during growth of the plates in the transverse direction [12, 13]. The condition for the reverse transformation is given by

$$-\Delta G_{ch}^{M-A} - \Delta G_{rev}^{M-A} + \Delta G_{ir}^{M-A} = 0. \quad (2)$$

Equations (1) and (2) show that the reversible energy opposes the growth and nucleation of martensite plates, but during the reverse transformation facilitates the reversion to austenite [14].

The transformation temperatures are related to T_0 by

$$M_s = T_0 - \frac{\Delta G_{ir}}{\Delta S_c} - \frac{\Delta G_{rev}^0}{\Delta S_c} \quad (3)$$

$$A_s = T_0 + \frac{\Delta G_{ir}}{\Delta S_c} - \frac{\Delta G^1_{rev}}{\Delta S_c} \quad (4)$$

$$M_f = T_0 - \frac{\Delta G_{ir}}{\Delta S_c} - \frac{\Delta G^1_{rev}}{\Delta S_c} \quad (5)$$

$$A_f = T_0 + \frac{\Delta G_{ir}}{\Delta S_c} - \frac{\Delta G^0_{rev}}{\Delta S_c} \quad (6)$$

where ΔG^0_{rev} is the reversible energy cost for the nucleation of martensite, ΔG^1_{rev} is the total reversible energy cost for the growth and nucleation of martensite, ΔG_{ir} is the dissipated energy of the transformation, and ΔS_c is the entropic change of transformation [15-17]. This assumes that the energy dissipation occurs only during nucleation and has the same value for both forward and reverse transformations. Thus, all of the transformation temperatures can be related to T_0, which is itself determined by chemistry, through measures of the dissipated and elastic energies of the system. Equation (3) and (6) show that the thermal hysteresis, $\frac{\Delta G_{ir}}{\Delta S_c}$, can be calculated by subtracting M_s from A_f.

1.3. Martensite twinning and variants

To understand the reversible energy contributions it is necessary to explain how elastic strain energy arises during the martensitic transformation and how the morphology of martensite accommodates this strain energy. During the martensitic transformation the atoms shift slightly from their positions in the parent lattice structure to new positions in the martensitic lattice structure. For example, Figure 1.2 shows the

lattice positions for atoms in an austenite FCC structure and their corresponding positions after transformation to the martensitic FCT structure.

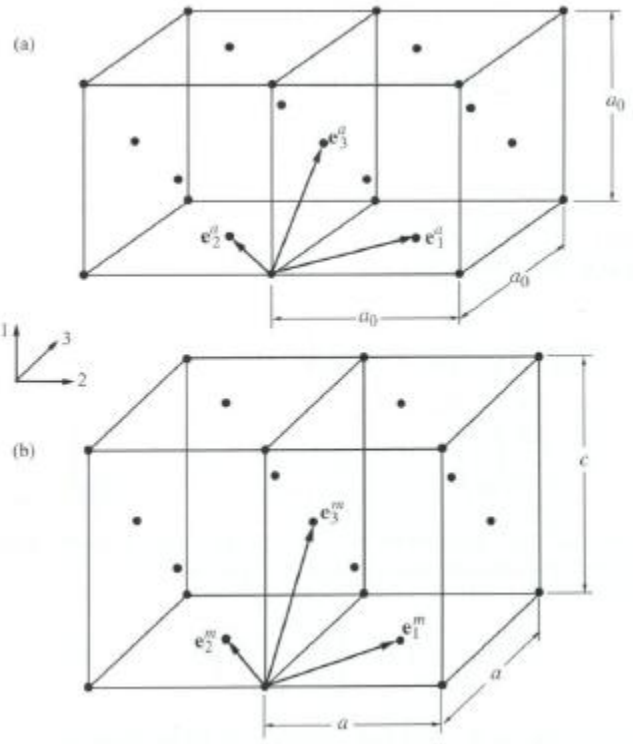

Figure 1.2 Schematic martensitic transformation from cubic austenite to tetragonal martensite. The lattice parameters change from a_0 to c in the 1 direction, and from a_0 to a in the second and 3 directions [18].

In this case, the forward transformation can be seen as an expansion in one direction and contraction in two directions. Due to the symmetry of this transformation, there are three variants of martensite that can form from the austenite; in this case, the expansion can occur in either the 1, 2, or 3 directions in Figure 1.2 [18].

To minimize the shear strain that necessarily accompanies the transformation shape change, martensite takes a twinned, self-accomodating morphology. These twin related, martensite variant pairs nucleate and grow together in such a way that helps to minimize the macroscopic transformation shear [3]. In a reversible (thermoelastic) transformation the remaining strain is accommodated elastically. Thus, the reversible energy term ΔG_{rev}^{A-M} represents the elastic strain energy that could not be relaxed by martensite morphology as well as the interfacial energy stored in the martensite/austenite and martensite/martensite interfaces [5].

1.3.1. The shape memory effects

The transformation route for the one-way shape memory effect begins with the material in a martensitic state; that is, multivariant, twinned, and self-accomodated. On the application of sufficient stress the processes of detwinning and reorientation occur; martensite variants in favorable directions to the applied stress grow at the expense of unfavorable variants [19]. If sufficient stress is applied a microstructure containing only a single variant of martensite can be obtained; this results in a macroscopic deformation. However, the deformation that results from detwinning and reorientation is completely reversed when the material transforms on heating to A_f. No further shape changes occur when the material is cooled to M_f, although the material returns to its original twinned martensite structure [20].

In the pseudoelastic effect reversible deformations occur on application of stress to an SMA above A_f. Figure 1.3 shows the dependency of the transformation

temperatures on applied stress. If a stress is applied at a temperature above A_f, the critical temperature for the nucleation of martensite increases. If the resistance of the matrix to slip dislocation is suitably high, variants of martensite favorable to the applied stress will nucleate and grow. When the stress is removed the martensite plates will become thermodynamically unstable and revert to austenite [3].

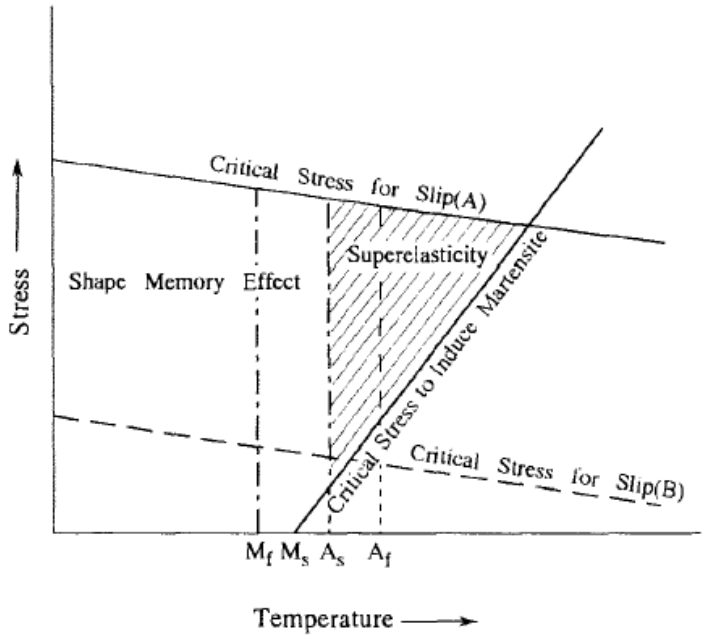

Figure 1.3 Typical stress temperature phase diagram for a shape memory alloy [3].

1.4. The shape memory effect in NiTi

NiTi is an intermetallic compound that forms in the Ni-Ti system when the Ni content is between 49-57% (at%) [21]. Its structure can take three distinct forms depending on the temperature; the CsCl B2 structure, the trigonal R phase, and the

monoclinic B19` structure [22]. Figure 1.4 shows the phase diagram for the NiTi system. The inset shows that to the Ni-rich side of the single phase NiTi boundary is a two-phase NiTi and Ni_4Ti_3 region. To the Ni-poor side is a NiTi and $NiTi_2$ two-phase region.

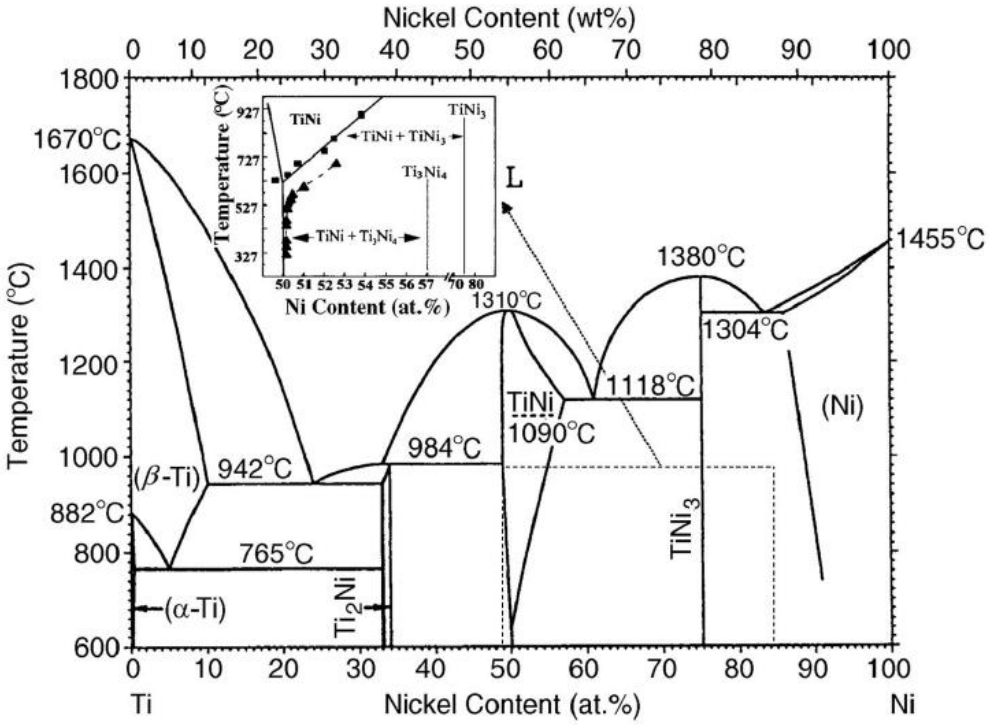

Figure 1.4 The Ni-Ti system phase diagram. The inset shows the Ni_4Ti_3 phase line [21].

Ni_4Ti_3 precipitates are of particular importance to NiTi alloys. Many studies have shown the effect on Ni_4Ti_3 precipitation on the martensitic transformation temperatures [16, 23-29], creep behavior [30, 31], multiple step transformations[32-40], R-phase transformation [24, 28], pseudoelastic behavior [27, 41-43], fracture behavior [44], fatigue behavior [45, 46], and internal friction during transformation [29].

The presence or absence of Ni_4Ti_3 precipitates also governs the transformation route in NiTi SMAs. In single phase NiTi, the B2 austenite transforms directly in to B19' martensite in the forward transformation and vice versa during the reverse transformation [2, 3]. However, when NiTi with a high Ni content (>50.5 at% Ni) is heat treated to form Ni_4Ti_3 precipitates, the forward transformation occurs in two steps; from B2 austenite to R-phase to B19' (and vice versa) [28, 47-54].

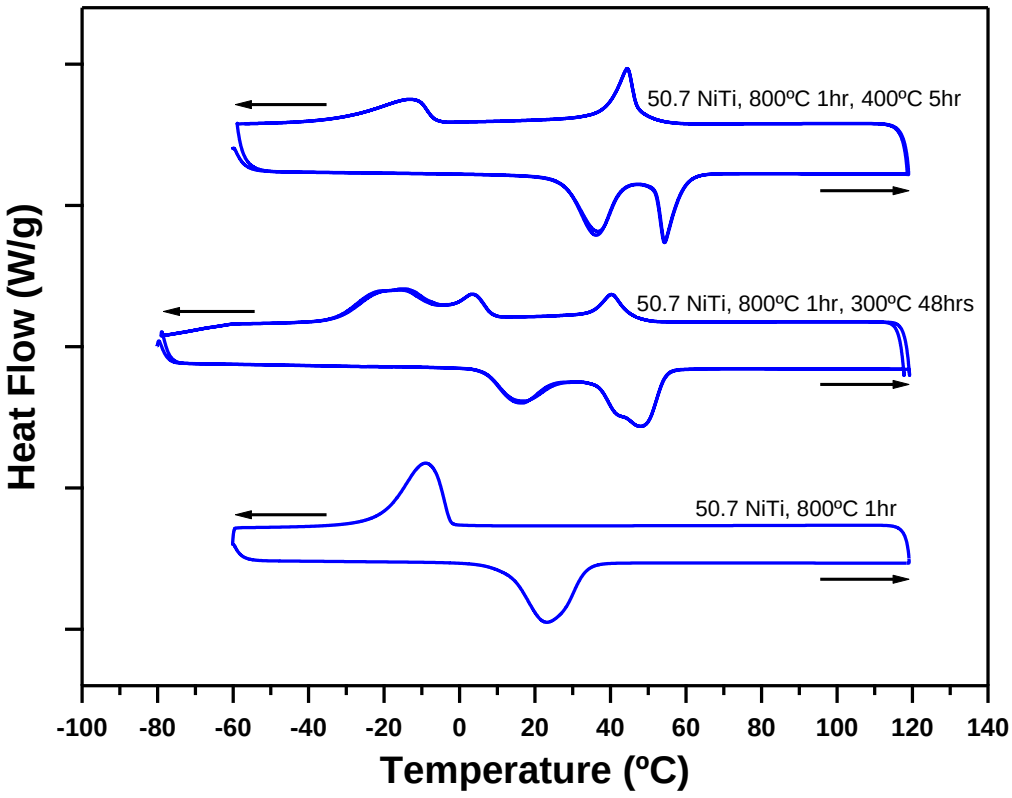

Figure 1.5 DSC curves for NiTi materials undergoing single step, R-phase, and multiple step transformations.

Under certain aging conditions Ni-rich NiTi alloys can also undergo transformations with more than two steps. These multiple-step transformations can be caused by a variety of mechanisms. Large scale inhomogeneities in the matrix due to preferential nucleation of Ni_4Ti_3 at the ground boundaries can occur during low duration, low temperature aging [35, 37, 53]. Ni_4Ti_3 precipitates are associated with local compositional gradients [35, 55] and coherency stresses [32, 56] which are favorable for nucleation of martensite plates. Under these conditions the precipitate-dense grain boundary regions transform at a different temperature than the precipitate-free grain interior. The multiple-step transformation has also been linked to large scale compositional gradients due to oxygen and hydrogen contamination during high-temperature heat treatments [50, 57]. Figure 1.5 shows differential scanning calorimetry (DSC) curves for NiTi materials with different aging treatments exhibiting the three different transformation paths.

It can also be seen in this figure that the thermal hysteresis of the B2-R transformation (A_f - M_s) is much smaller than that of the B2-B19' and R-B19' transformations. The B2-R transformation is also associated with a transformation strain an order of magnitude smaller than that of the B2-B19' and R-B19' transformations [2, 28].

1.5. Effect of precipitation on the transformation temperatures

Figure 1.6 shows the time-temperature-transformation diagram for a NiTi alloy with a 52 (at%) Ni concentration. Ni_4Ti_3 forms at aging temperatures below 900K.

Depending on the aging conditions the precipitates can form either homogenously or preferentially at the grain boundaries [58].

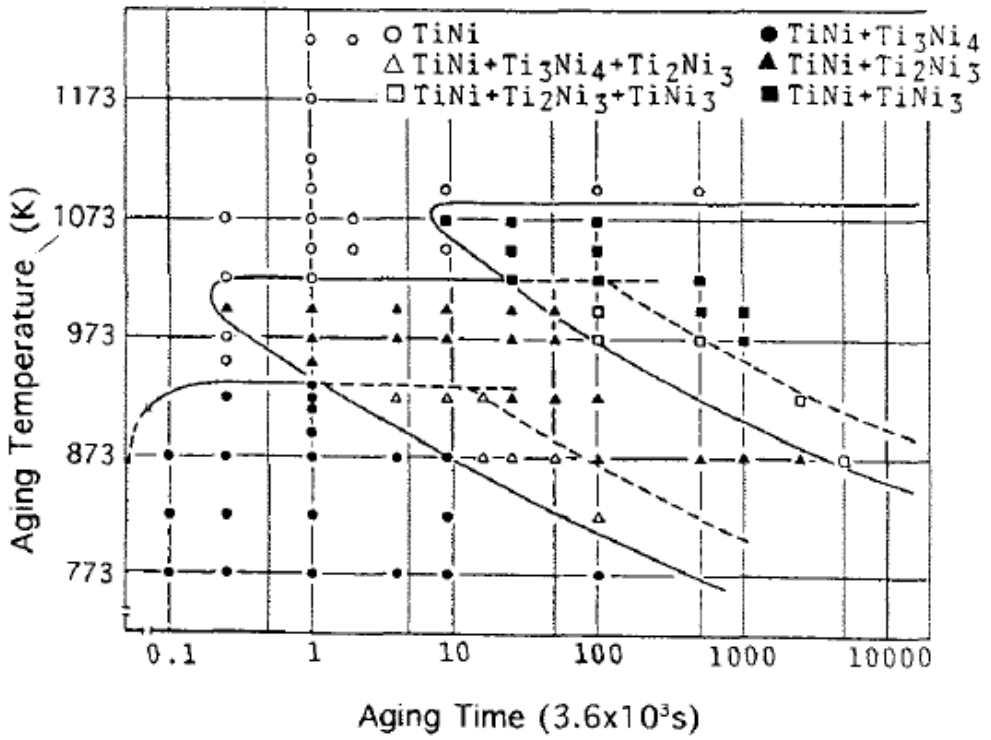

Figure 1.6 The time-temperature-transformation diagram for a 52 (at%) NiTi alloy [3].

The martensitic transformation temperatures are highly dependent on the chemistry, microstructure, and thermodynamical state of a NiTi alloy. When Ni_4Ti_3 precipitates form from the matrix, the reversible and dissipative energies that arise during the martensitic transformation change from the single-phase case [16]. These energies determine the transformation temperatures. Figure 1.7 shows schematically how the reversible and dissipated energies affect all of the transformation temperatures for a

material with a constant T_0. In a), only the chemical gibbs free energy is considered and the transformations begin and end at the same temperature. In b), both the chemical and dissipated energy contributions are considered; in this case the dissipated energy causes undercooling below T_0 and superheating above T_0; the amount of cooling/heating is equal in both directions. The transformations begin and end at a single temperature.

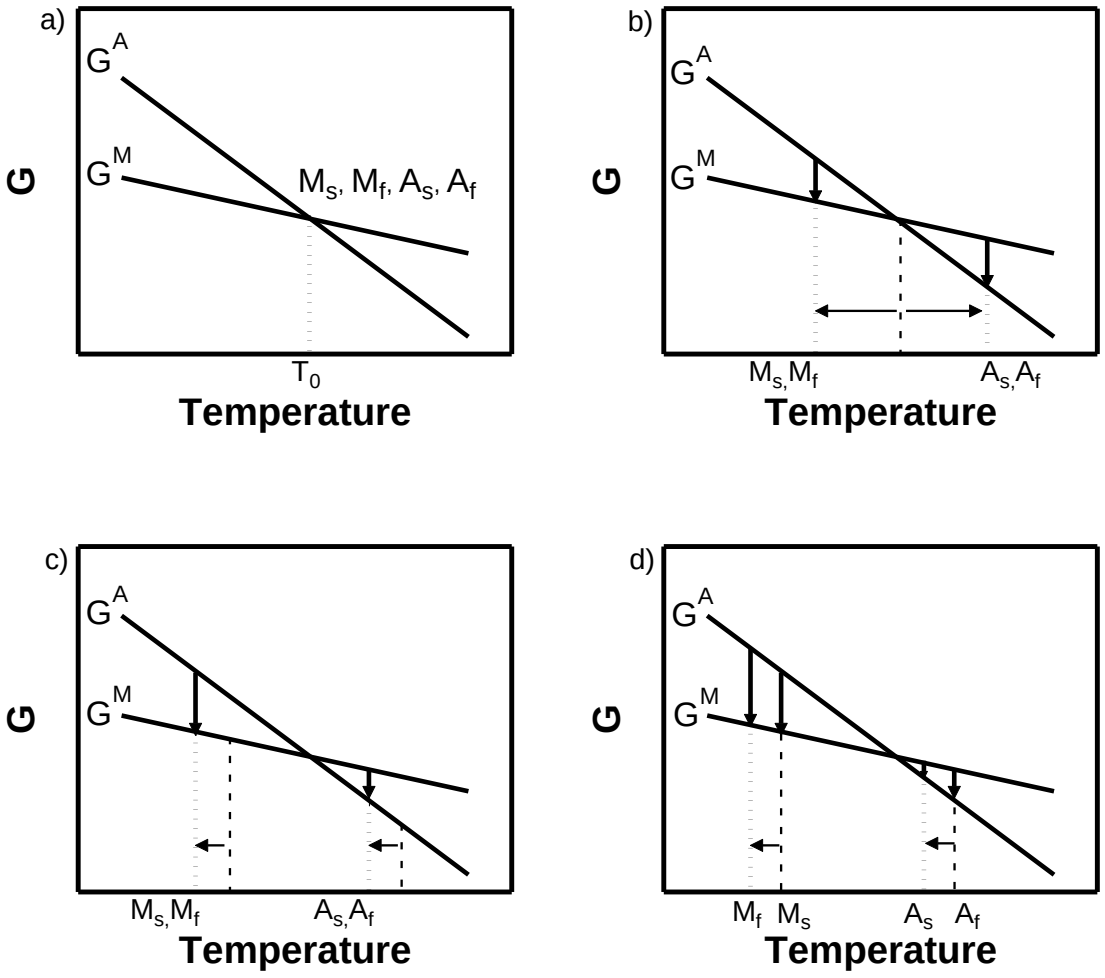

Figure 1.7 Schematic Gibbs free energy curves of an SMA showing the effect of reversible and irreversible energy contributions to the transformation temperatures: a) ideal case where ΔG depends only on ΔG_{ch}; b) case with ΔG_{ch} and ΔG_{ir}; c) ΔG_{ch}, ΔG_{ir} and ΔG_{rev}^{0}; d) ΔG_{ch}, ΔG_{ir}, ΔG_{rev}^{0} and ΔG_{rev}^{1}

In c), the reversible energy during nucleation is considered. The transformation temperatures are all decreased an equal amount; however, the transformations still begin and end at a single temperature. In d) the reversible energy during growth is considered. M_s and A_s remain unchanged, but now the transformation requires additional undercooling to continue and complete the growth of martensite plates.

If T_0 is changed, all of the transformation temperatures will shift by an amount equal to the change in T_0. T_0 is highly dependent on the ratio of Ni to Ti. As the Ni content increases, T_0 decreases, going from 370K for an equiatomic Ni-Ti ratio to 255K at 50.7 at% Ni [59]. During aging treatments, the precipitation of Ni-rich Ni_4Ti_3 particles lowers the overall matrix Ni composition, changing the T_0 of transformation.

The M_s temperature is then also highly dependent on the Ni content due to its relation to T_0. Figure 1.8 shows that M_s remains relatively constant when the Ni content is below 49.5 at%. As the Ni content increases, M_s decreases until the martensitic transformation is completely suppressed [60].

Changes in the composition also affect the compatibility between the austenite and martensite phases. According to the theory of Ball and James, this compatibility can be measured by λ_2, the second ordered eigenvector of the tensor which describes the transformation strain for the martensitic transformation [61]. A transformation with λ_2 equal to 1 has a direction at the austenite/martensite interface in which there is no stretching; in this case a single variant of martensite is sufficient to minimize the elastic and interfacial energy of the interface, and the hysteresis is significantly lowered [62]. In NiTi, λ_2 increases with composition.

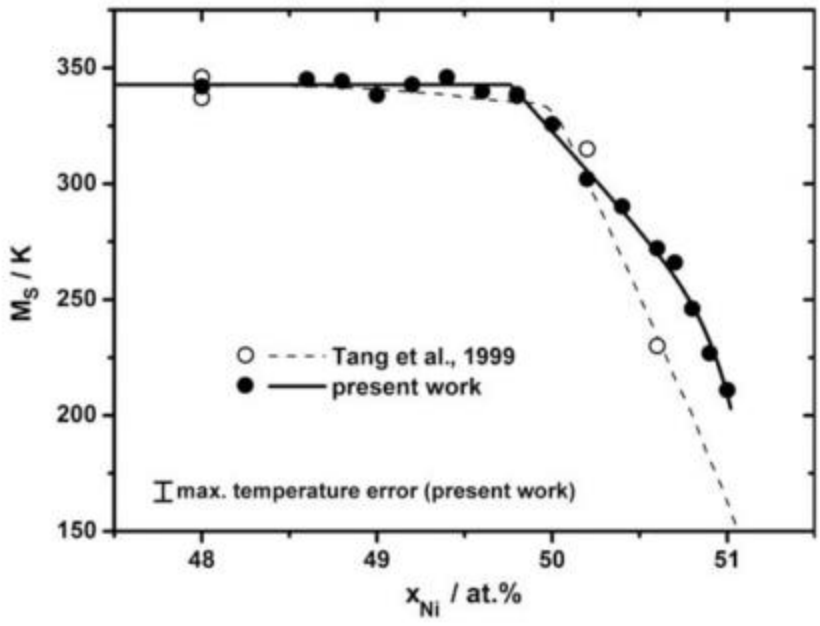

Figure 1.8 Dependence of M_s temperature on Ni content [60].

Figure 1.9 shows that in NiTi, the λ_2 parameter approaches 1 as the Ni content increases. This is matched by a corresponding decrease in thermal hysteresis as the compatibility of the martensite improves [60].

The distance between precipitates has a large effect on the reversible energy stored during transformation. [16, 63, 64]. When the material is composed of a single phase, or the interparticle distance is sufficiently large, the martensite morphology is made up of type I and type II twins. However, as the interparticle distance decreases the twinning type changes to compound twins which are finer and denser [63, 65]. The increase in twin density is accompanied by an increase in reversible interfacial energy, which decreases both the M_s and A_s [16].

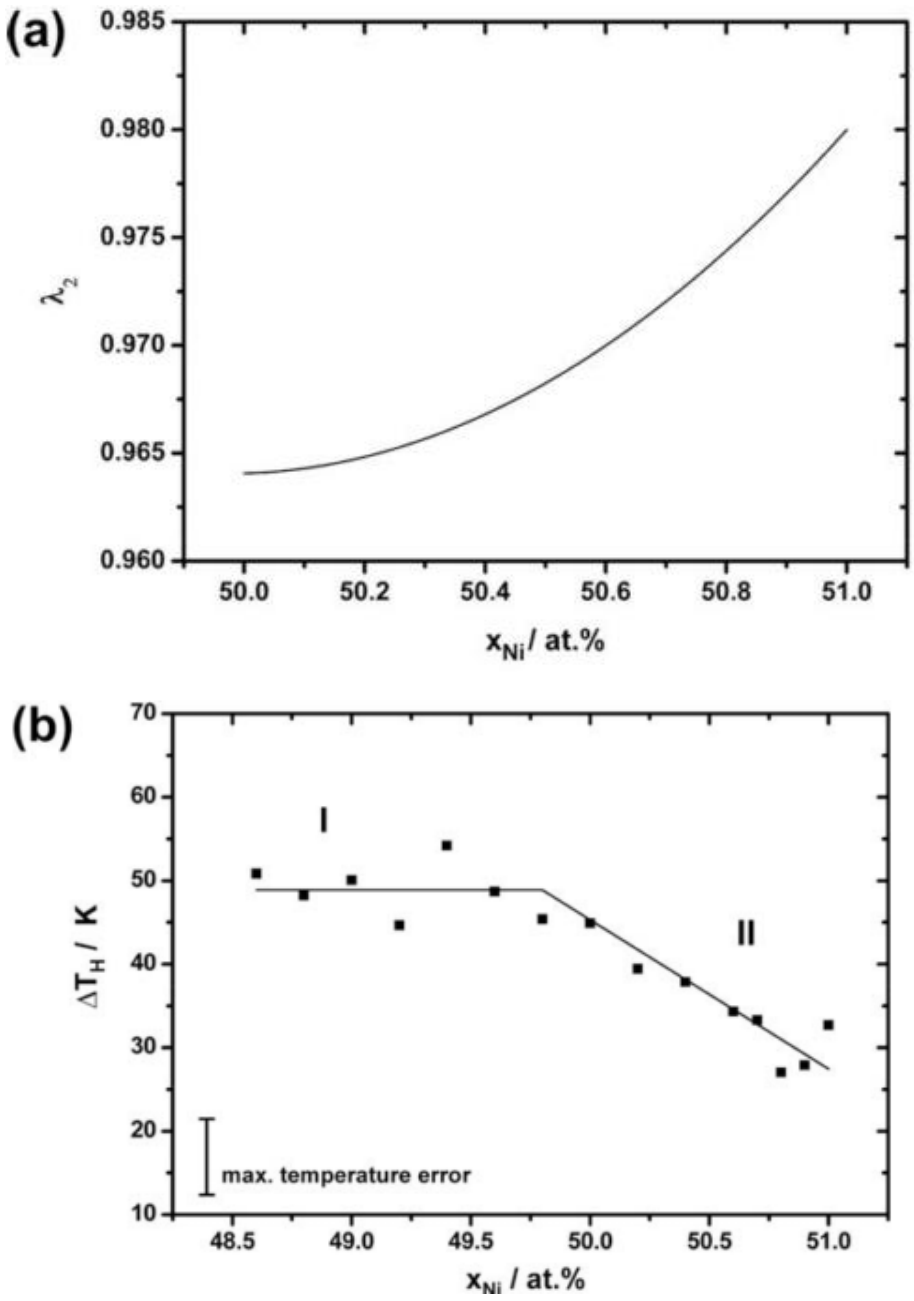

Figure 1.9 Relationship between λ_2, thermal hysteresis, and Ni content in NiTi SMAs. a) Dependence of Austenite/martensite compatibility factor λ_2 on Ni content. b) Dependence of thermal hysteresis on Ni content [60].

Additionally, if the interparticle distance is below the critical nucleation radius for the formation of a martensite plate, an additional reversible energy barrier appears, further suppressing M_s [64].

These same effects appear in polycrystalline materials with small grain sizes; as the grain size decreases the twinning type changes from type I and type II to dense compound twins, accompanied by an increase in reversible energy during transformation [16].

During the transformation, energy is dissipated through two different mechanisms: resistance to interfacial motion, and generation of defects [5, 7, 10, 11]. If the material is sufficiently strong, then defect generation becomes difficult, and the transformation temperatures become very stable with successive cycling. Additionally, high matrix strength increases the resistance to interfacial motion [66]. The strength of the matrix is governed by two competing mechanisms; these are the strength due to supersaturation of Ni (solid solution strengthening) and the strength due to precipitation (precipitation hardening). When Ni-rich NiTi is aged and Ni_4Ti_3 precipitates form, the solid solution strengthening becomes less effective (due to the reduction in Ni supersaturation) while precipitation hardening initially strengthens the material and then becomes less effective as precipitates become larger and incoherent [67].

Precipitates in a transforming material can themselves store reversible elastic energy as long as they do not transform and remain coherent with both the austenite and martensite phases [66, 67]. If the volume fraction of precipitates increases, then the amount of reversible energy stored in the precipitates will increase.

1.6. Objectives

Aging treatments are an effective and low-cost tool for modifying the transformation temperatures and hysteresis in NiTi alloys. Many studies have investigated the effect of low duration aging on the transformation temperatures [24, 58] and thermal hysteresis [16]. For engineering applications of NiTi SMAs more data on the effect of aging on the transformation temperatures and hysteresis is necessary. For actuator applications a small hysteresis may be desirable, to decrease the response time. In fastening applications a large hysteresis may be required, in order to widen the range of environments in which the material may be used without early transformation. Additionally, knowledge of the effect of aging on the transformation temperatures is necessary since engineering applications will specify the transformation temperatures at a certain range. To this end, the effect of aging treatments with a wide range of durations and temperatures are investigated.

In this work the following questions will be addressed using a systematic study:

- Under what conditions can high hysteresis be obtained?
- Under what conditions can low hysteresis be obtained?
- What are the transformation temperatures under high and low hysteresis conditions?
- What are the trends in the evolution of the hysteresis with respect to aging temperature and time?
- What are the trends in the evolution of the transformation temperatures with respect to aging temperature and time?

2. EXPERIMENTAL PROCEDURES

2.1. Sample preparation

Polycrystalline ingots with nominal compositions of 50.7, 50.9, and 51.5 (at%) Ni, with balance Ti, were obtained from commercial vendors. The 50.7 NiTi material was received in a hot rolled condition, the 50.9 NiTi material was hot extruded in a mild steel can, and the 51.5 NiTi material was received in an as-cast condition. Bars with a diameter of 2.5mm were cut from the ingots using electrostatic discharge machining (EDM). The bars were first mechanically ground to remove the rough EDM surface layer. Each bar was then wrapped in Kanthal (FeCrAl) wire to prevent any reaction with the quartz tubing used in aging and solution treatments. The air in each tube was evacuated five times using a pumping system, and then sealed under an ultra high purity argon atmosphere. Solution heat treatments were performed to promote sample homogeneity, to reduce residual stresses, and to eliminate secondary phases. After each solution treatment the samples were quenched into water. The composition, solution treatment duration, and solution treatment temperature for each material are given in Table 2.1. Back scatter electron imaging (BSE) was used to examine material to ensure a uniform grain size, precipitate condition, and microstructure.

Table 2.1 Nominal compositions, solution treatment temperatures and durations for polycrystalline binary NiTi samples

Nominal Ni Composition (at%)	Solution treatment temperature (ºC)	Solution treatment duration (hrs)
50.7	800	1
50.9	900	1
51.5	900	24

2.2. Aging treatments

After solution treatments the materials had a polycrystalline structure with a single phase matrix. In some cases small numbers of TiC precipitates remained near the grain boundaries; the source of these precipitates was believed to be the use of graphite crucibles during the initial melts. From each solution treated bar small 50mg DSC samples were cut using a diamond impregnated sectioning blade. Each DSC sample was wrapped in Kanthal wire and sealed under an argon atmosphere into a quartz tube. Systematic aging heat treatments were performed to investigate the effect of Ni_4Ti_3 precipitates on the transformation temperatures and the hysteresis of these materials. Table 2.2 shows the temperature and duration of the aging treatments applied to each material composition. Additional low temperature aging treatments were performed for the 50.9 and 51.5 NiTi materials, but did not show any transformation and so are not listed in this table. After each aging treatment the samples were quenched into water.

Table 2.2 Aging treatments and durations used to investigate the effect of Ni_4Ti_3 precipitate formation on transformation temperature and hysteresis

Aging Temperature	Aging Durations	Nominal Ni Content (at%)
200	0.5, 1, 3, 5, 10, 24, 48, 72, 100	50.7
300	0.5, 1, 3, 5, 10, 24, 48, 72, 100	50.7
350	0.5, 1, 3, 5, 10, 24, 48, 72, 100	50.7, 50.9
375	24, 48, 72, 100	50.9, 51.5
400	0.5, 1, 3, 5, 10, 24, 48, 72, 100	50.7, 50.9, 51.5
425	0.5, 1, 3, 5, 10, 24, 48, 72, 100	51.5
450	0.5, 1, 3, 5, 10, 24, 48, 72, 100	50.7, 50.9, 51.5
500	0.5, 1, 3, 5, 10, 24, 48, 72, 100	50.7, 50.9, 51.5

2.3. Differential scanning calorimetry experiments

After the aging treatments DSC experiments were performed to determine the transformation temperatures of the material. The DSC samples were mechanically polished to ensure that the outer layers were free of any oxidation. These experiments were performed using a QA instruments Q20 DSC. Each sample was first cooled to -80ºC, and then cycled twice between -80ºC and 120ºC using a heating-cooling rate of 10ºC/minute.

The heat flow measurements taken by the DSC were used to determine the transformation temperatures of each sample. Figure 2.1 shows a typical DSC measurement for an SMA. The arrows indicate the directions on the plot for cooling and heating. The transformation temperatures were determined using the tangent method.

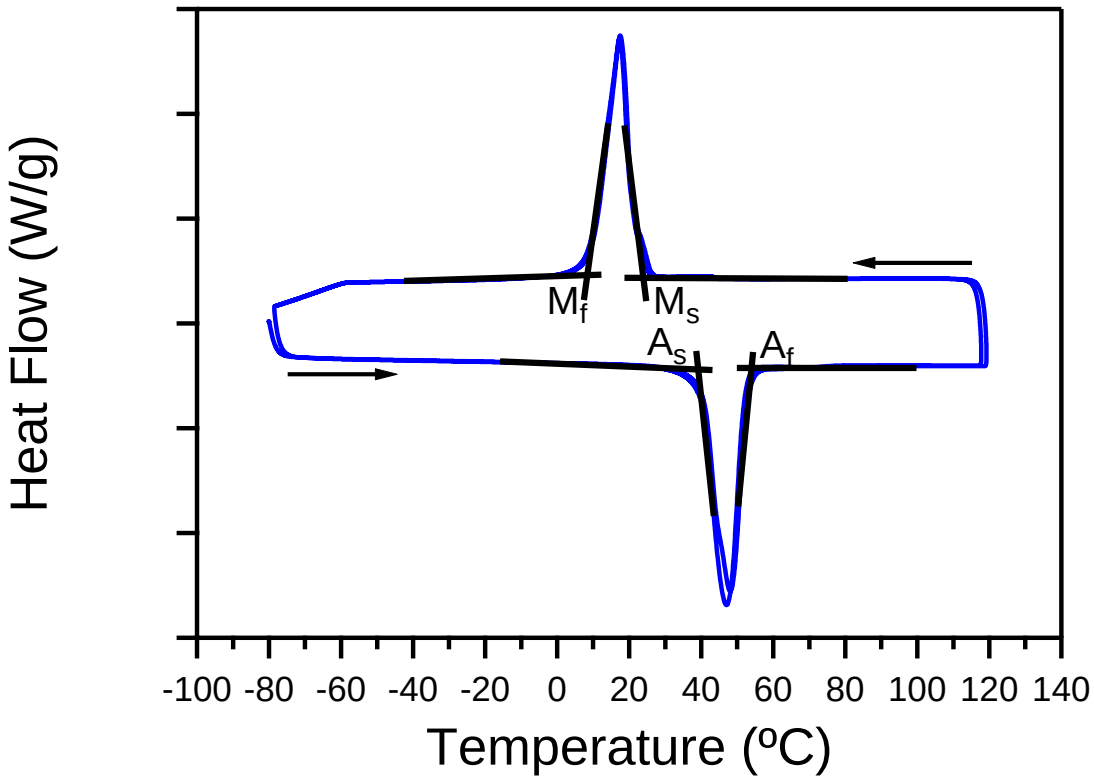

Figure 2.1 Schematic heat flow temperature response of an SMA showing determination of the transformation temperatures using tangent method.

In aging conditions where single peak transformations were observed, the transformation temperatures correspond to the B2-B19' transformation. In aging conditions where multiple-step transformations were observed, the transformation temperatures for the largest enthalpy peaks were selected. For aging conditions with an intermediate R-phase transformation, the transformation temperatures for the R-B19' transformations were selected. In cases where the B19'-R and R-B2 transformations occurred concurrently, the A_f temperature corresponds to the R-B2 transformation finish temperature.

2.4. Optical and scanning electron microscopy

Optical and scanning electron microscopy (SEM) were performed at various stages throughout the experimental procedure. Optical microscopy was performed using a Keyence VH-Z100 digital microscope. Analysis of the grain size, microstructure, and phase morphology was performed using a Cameca SX50 SEM. Determination of the chemical composition of the samples and of the secondary phases was performed using wavelength dispersive X-ray spectrometry (WDS) and energy-dispersive X-ray spectrometry (EDS).

Table 2.3 shows the results of WDS compositional analysis and DSC transformation temperatures. The WDS results are known to have an intrinsic bias error; so they were compared against DSC measurements to give an idea of degree of bias. The nominal 50.4 (at%) Ni material was measured using WDS to have a 50.67 (at%) Ni content using WDS, but from DSC measurements of the M_s temperature the composition is expected to be 50.9 (at%) Ni. The nominal 51.2 (at%) Ni material was measure using WDS to have a 50.52 (at%) Ni content, but from DSC the composition is expected to be 50.9 (at%) Ni. From comparisons of all the compositions, the bias is estimated to be in the range of 0.3-0.5 (at%) Ni. The 50.7 (at%) Ni material is estimated to have a true 50.7 (at%) Ni concentration, while the 50.9 (at%) Ni material concentration is in the range of 51.1-51.4 (at%) Ni, and the 51.5 (at%) Ni material concentration is in the range of 52.5-52.6 (at%) Ni.

Table 2.3 WDS compositional analysis results for various studied NiTi materials with various Ni concentrations. Transformation temperatures measured using DSC are shown for comparison. Compositions selected for this studied are highlighted in grey.

Ni Content (at%)				
Nominal	WDS	Ms (Expected)	Ms (Actual)	DSC Composition
50.4	50.67	-11ºC	-38ºC	50.9
50.7	50.36	15ºC	-2ºC	50.7
50.9	50.89	-41ºC	<-80ºC	>51.1
51.1	50.71	-21ºC	<-80ºC	>51.1
51.2	50.52	5ºC	-33ºC	50.9
51.5	52.12	-59ºC	<-80ºC	>51.1

3. EFFECT OF AGING ON THE TRANSFORMATION TEMPERATURES

3.1. The M_s temperature

The M_s temperatures for the 50.7 (at%) NiTi material aged at various temperatures and durations are shown in Figure 3.1. Under solution heat treated conditions the M_s temperature is -2ºC. After subsequent aging at 200ºC the M_s temperature initially remains relatively constant, but begins to decrease after 10 hours of aging.

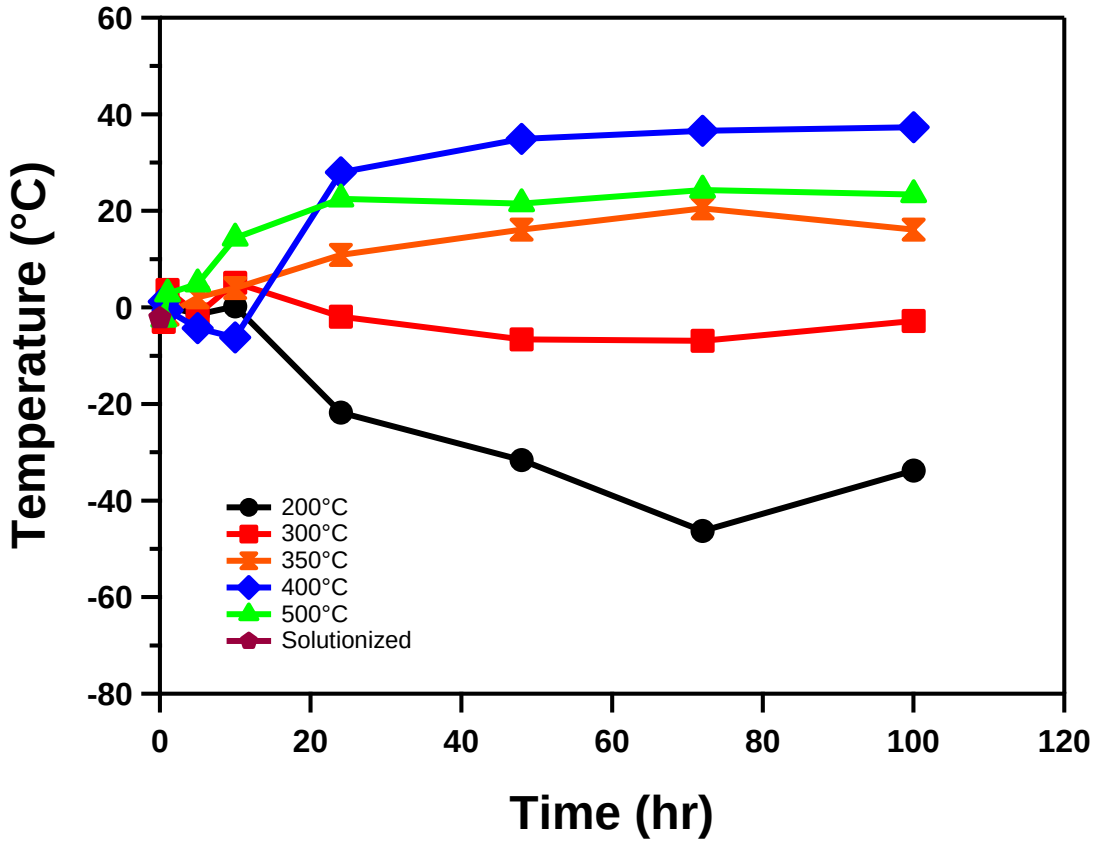

Figure 3.1 M_s temperatures for 50.7 (at%) NiTi after aging

During aging from 10-72 hours the M_s temperature decreases with additional aging, reaching a minimum of -46ºC. After 72 hours the trend reverses; subsequent aging increases the M_s temperature to -33ºC at 100 hours. The trend during aging at 300 ºC is similar, however the M_s reduction is smaller in magnitude.

When the aging temperature is increased to 350ºC the M_s temperature begins to increase with subsequent aging; from 0.5 to 72 hours the M_s increases by 22ºC; additional aging to 100 hours reduces the M_s temperature by 5ºC. During 400ºC aging there is a slight decrease in M_s temperatures from 0.5 to 10 hours. Additional aging to 24 hours increases M_s by 34ºC, and as the aging time approaches 100 hours the M_s temperature saturates at 37ºC. At the highest aging temperature (500ºC) the M_s temperature begins to increase immediately on aging, and reaches its saturation after 24 hours of aging.

As the aging temperatures increased from 200ºC to 400ºC the average M_s temperatures increased as well. The lowest M_s temperature is obtained through aging at 200ºC, while the highest is obtained through aging at 400ºC. The M_s temperatures decrease when the aging temperature increases from 400ºC to 500ºC.

Figure 3.2 shows the M_s temperatures for the 51.2 (at%) NiTi material aged at various temperatures and times. For this material the transformation temperatures for the solutionized material are below the lower limit of the DSC temperature cooling range (-80ºC) and therefore could not be detected. After aging below 350ºC no transformations are detected.

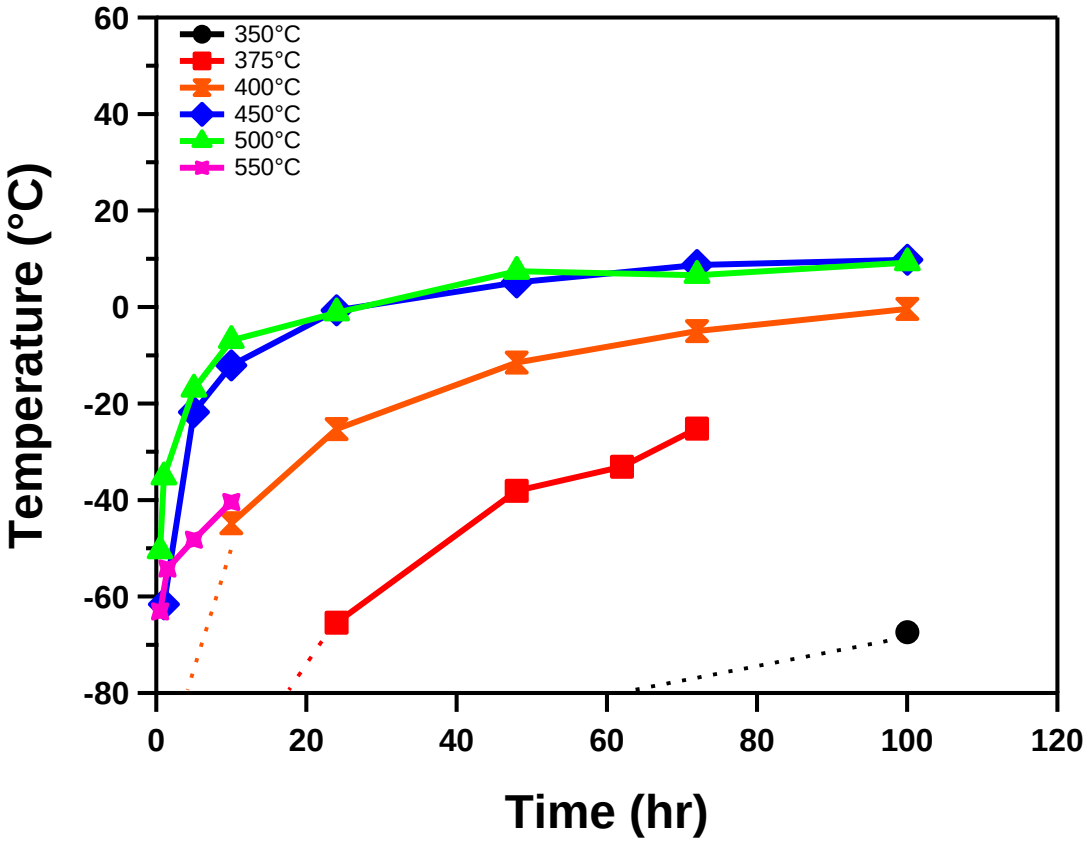

Figure 3.2 M_s temperatures for 51.2 (at%) NiTi after aging. Dashed lines indicate that the M_s temperature is below -80ºC and beyond the temperature limit of the DSC equipment

Aging the material for 100 hours at 350ºC yields the lowest M_s temperature (-67ºC) for this composition. When aged at 350ºC for less than 100 hours no transformations are detected; the dashed line in the figure indicates that the M_s temperature is below -80ºC for a 72 hour heat treatment.

When the aging temperature is increased to 375ºC transformations are detected for aging durations at 24 hours and above. When aged at 400ºC transformations are

detected for aging durations at 10 hours and above; for 450ºC at 1 hour and above. For aging at 500ºC and 550ºC transformations are observed for all durations.

At any given aging temperature only increases in M_s with subsequent aging are observed. However, because of the -80ºC lower limit of the DSC equipment it is possible that a decreasing trend exists after very short duration aging. The M_s curves for 400ºC and below continue to increase until 100 hours of aging is reached; but the M_s temperatures for 450ºC and 500ºC saturate after 72 hours of aging. Additionally as the aging temperature increases the concavity of the curves also increase.

The M_s temperature increases with aging temperature from 350ºC to 450ºC; however, from 450ºC to 500ºC there is very little change in M_s. When the aging temperature is further increased to 550ºC the M_s temperatures decrease.

Figure 3.3 shows the M_s temperatures for the 52.5 (at%) NiTi material aged at various temperatures and times. When aged below 375ºC no transformation is detected; again, this indicates that the M_s temperature for these conditions is below -80ºC. For aging at 375ºC no transformation is detected below 72 hours of aging, for aging at 400ºC no transformation is detected below 10 hours of aging, for aging at 425ºC no transformation is detected below 1 hours of aging, and for aging at 450ºC no transformation is detected below 5 hours of aging. Samples aged at 500ºC show transformation at and above 0.5 hours of aging.

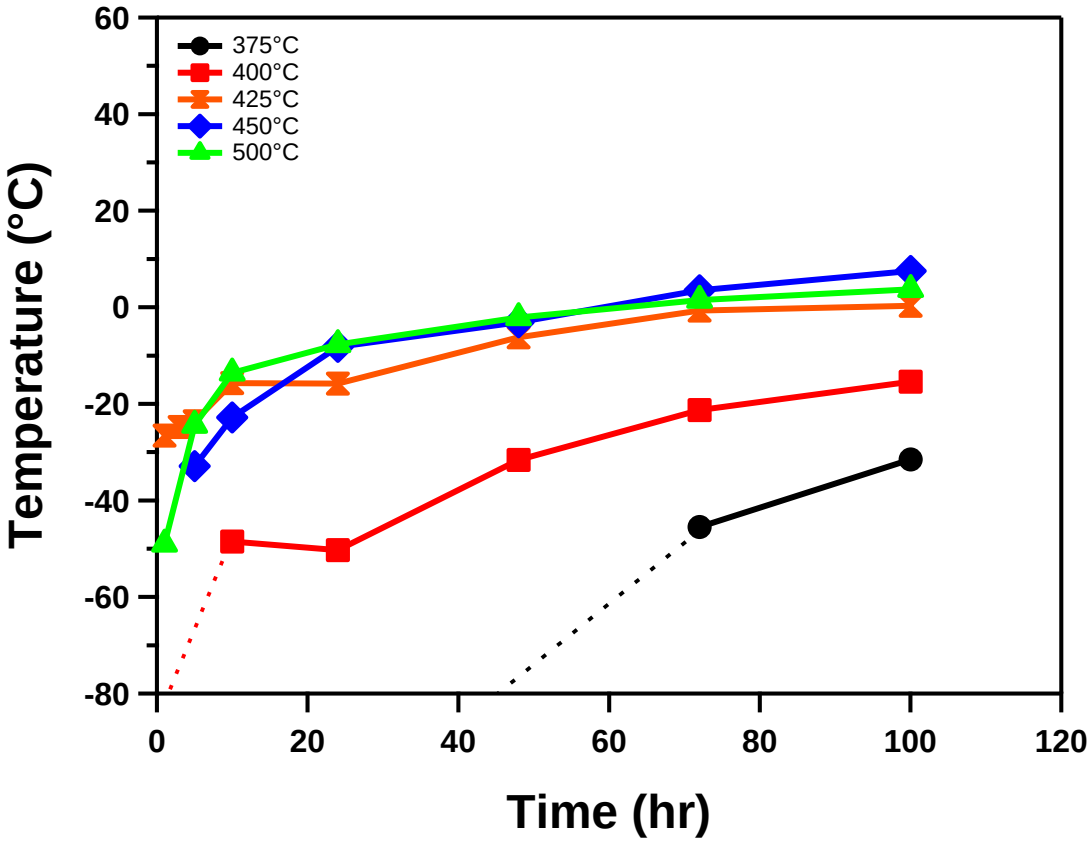

Figure 3.3 M_s temperatures for 52.5 (at%) NiTi after aging

Similarly to the 51.2 (at%) NiTi material only increases in M_s with subsequent aging are observed. The only exception was aging under 400ºC from 10 to 24 hours. Again, it is possible that decreasing trends are present with short duration aging, but cannot be observed because the M_s temperatures are extremely low. At all aging temperatures no saturation behavior was observed; even after 100 hours of aging the M_s temperatures continue to increase.

As the aging temperature increases from 375ºC to 450ºC the M_s temperatures increase as well, except for aging at 425ºC up to 10 hours, which yields higher M_s temperatures than aging at 450ºC. When the aging temperature is increased from 450ºC to 500ºC the M_s temperatures are higher until 24 hours of aging. From 24 hours to 48 hours they are the same, and from 72 to 100 hours aging at 500ºC yields lower M_s temperatures. Additionally the concavity of the M_s curves increases as the aging temperature increases.

3.2. The R_{sr} temperature

Figure 3.4 shows the R_{sr} temperatures for the 50.7 (at%) NiTi material aged at various temperatures and durations. At lowest aging temperature (200ºC) the R_{sr} temperature remains within 2º of that of the solution treated condition for up to 10 hours of aging. Further aging to 24 hours reduces the R_{sr} temperature by 22º; subsequent aging to 100 hours yields only small changes in R_{sr}. No significant reduction in R_{sr} is observed in aging temperatures above 200ºC.

When the aging temperature is increased to 300ºC and 350ºC the R_{sr} temperatures increase from 0.5 to 24 hours. From 24 to 100 hours of aging at 300ºC the changes in R_{sr} are small in magnitude, while at 350ºC the R_{sr} increases by 10ºC.

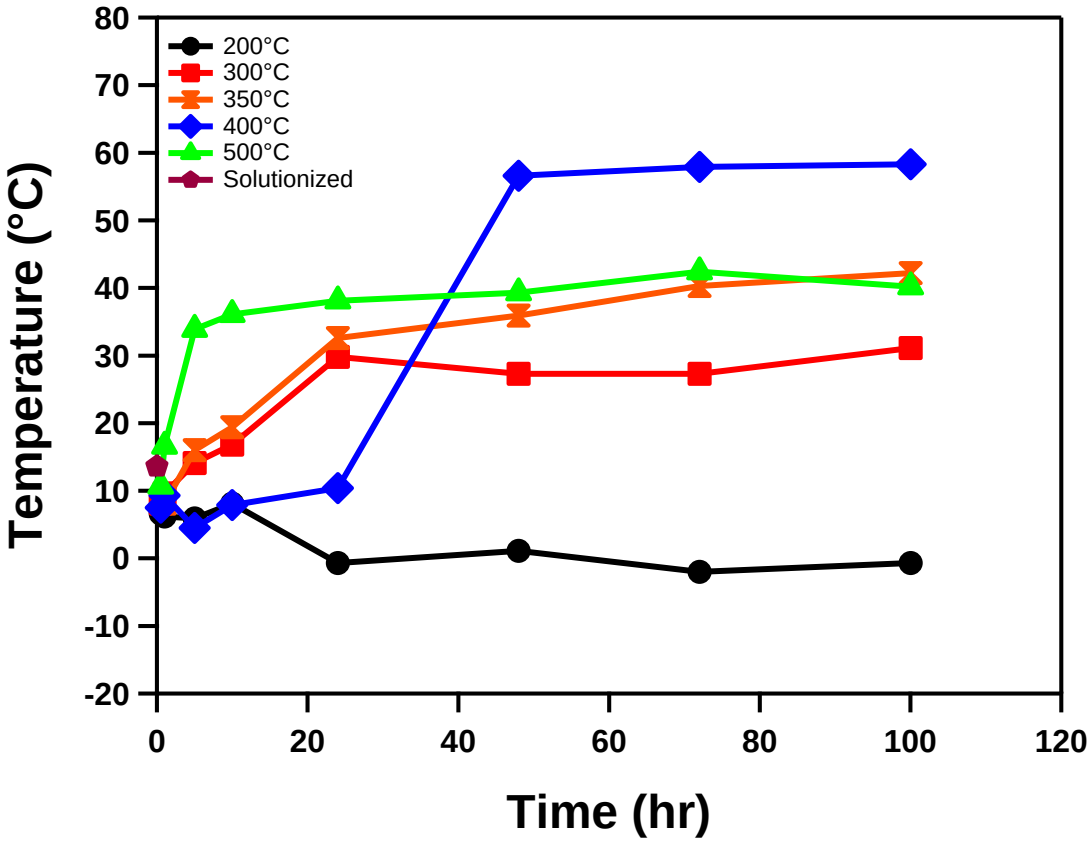

Figure 3.4 R_{sr} temperatures for 50.7 (at%) NiTi after aging

Aging at 400ºC from 0.5 to 24 hours yield an increase in R_{sr} which is smaller than that seen in aging at 300ºC and 350ºC. Further aging from 24 to 48 hours leads to an increase in R_{sr} of 46ºC. This trend was not seen in any other aging treatment applied to this material. Subsequent aging from 48 to 100 hours does not change the R_{sr} temperatures significantly. At the highest aging temperature (500ºC) the R_{sr} temperature increases immediately on aging, and the rate of increase is higher than any of the other heat treatment conditions investigated. From 5 hours to 72 hours the R_{sr} temperature

changes moderately with aging time; from 72 hours to 100 hours a slight decrease in R_{sr} is observed.

The lowest R_{sr} temperature is obtained after aging at 200ºC, while the highest was obtained by aging at 400ºC. As the aging temperature increases from 200ºC to 350ºC the R_{sr} temperatures increase; however, when the aging temperature increases from 350ºC to 400ºC the R_{sr} temperatures are lower for 400ºC aging with short duration aging (0-24 hours) but higher for long duration aging (48-100 hours). When the aging temperature increases from 400ºC to 500ºC the R_{sr} temperatures increase for short duration but decrease for long duration aging.

Figure 3.5 shows the R_{sr} temperatures for the 51.2 (at%) NiTi material aged at various temperatures and durations. No transformation is observed for aging treatments below 350ºC. When the aging temperature is 350ºC no transformation is observed until 100 hours. After aging at 375ºC transformation is observed for 24 hours and above; at 400ºC for 10 hours and above; at 450ºC for 1 hour and above, and for 500ºC for 0.5 hours and above. It is important to note that the R_{sr} temperatures under these conditions may be actually be higher than -80ºC; however, since the corresponding M_s temperatures are below the limit of the equipment neither the forward nor the reverse transformation occurs during DSC experiments.

In all of the aging temperatures surveyed only increases in R_{sr} with subsequent aging are observed. As the aging temperature increases the slopes of the R_{sr}-aging time curves decrease. Unlike the 50.7 (at%) NiTi material no saturation behavior is observed, and even at the highest aging temperature (500ºC) the R_{sr} temperature continues to

increase with subsequent aging from 72-100 hours. As the aging temperature increases the concavity of the curves increase as well.

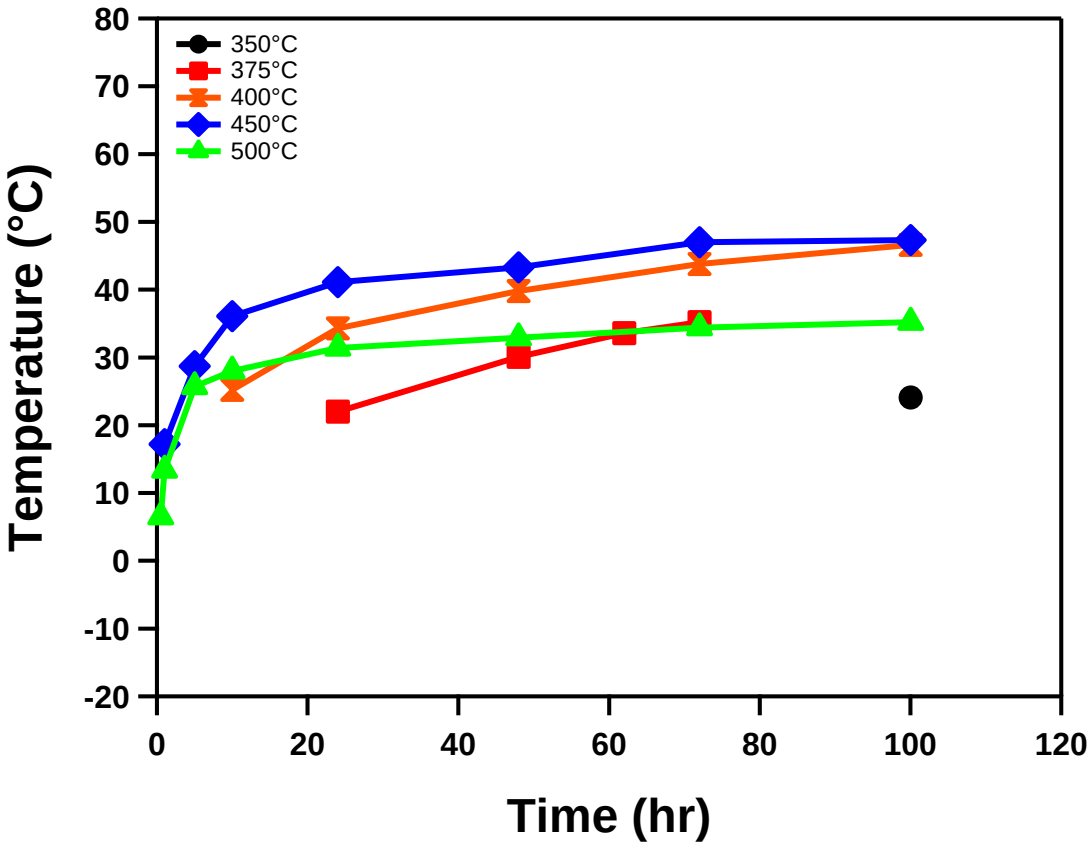

Figure 3.5 R_{sr} temperatures for 51.2 (at%) NiTi after aging

As the aging temperature increases from 350ºC to 450ºC the R_{sr} temperature increases; but when the aging temperature increases from 450ºC to 500ºC the R_{sr} temperature decreases. The highest aging temperature is obtained by aging at 400ºC for 100 hours, and the lowest by aging at 500ºC for 0.5 hours.

Figure 3.6 shows the R_{sr} temperatures for the 52.5 (at%) NiTi material aged at various temperatures and durations. No transformations are observed when aging at 375ºC below 48 hours; at 400ºC below 5 hours, and at 425ºC below 1 hour.

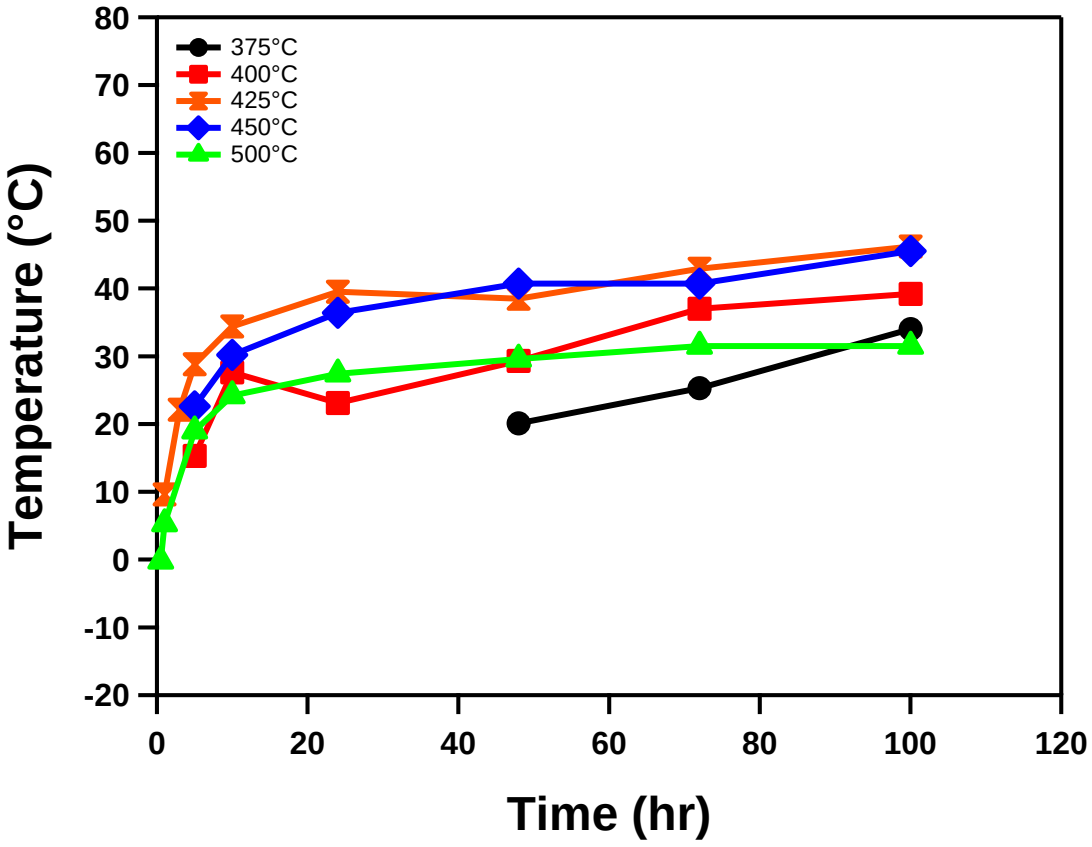

Figure 3.6 R_{sr} temperatures for 52.5 (at%) NiTi after aging

In general the R_{sr} temperatures increase with subsequent aging; the exceptions are aging at 400ºC for 10 to 24 hours and aging at 425ºC for 24 to 48 hours. Just as in the 51.2 (at%) NiTi the R_{sr} temperature-aging time curves become less steep as the aging

temperature increases. In addition to this the concavity of the curves increase as the aging temperature increases.

As the aging temperature increases from 375ºC to 425ºC the R_{sr} temperatures increase. From 425ºC to 450ºC there is little change in R_{sr}, and from 450ºC to 500ºC the R_{sr} temperature decrease. The lowest aging temperature was obtained by aging at 500ºC for 0.5 hours, and the highest was obtained by aging at 425ºC for 100 hours.

3.3. The A_f temperature

Figure 3.7 shows the A_f temperatures for the 50.7 (at%) NiTi material aged at various temperatures and durations. At the lowest aging temperature (200ºC) there is some deviation from the trend established for the M_s and R_{sr} temperatures. Initially the A_f temperature decreases, but from 10-24 hours it increases. From 24 to 48 hours there is a slight increase (1ºC), from 48 to 72 hours the A_f decreases, and from 72 to 100 hours it increases by 2ºC.

When the aging temperature is 300ºC the A_f temperature increases monotonically from 0.5 to 10 hours; further aging yields only small changes in A_f. Under aging at 350ºC the A_f temperature increases monotonically until 72 hours of aging; further aging yields only a 1º decrease in A_f. At 400ºC the same anomalous behavior seen in the M_s and R_{sr} temperatures is observed; initially, the R_{sr} temperature decreases from 0.5 to 10 hours. Further aging to 24 hours yields a large increase of 43º, and continued aging to 100 hours yields less pronounced increases in A_f. At the highest

aging temperature (500ºC) the A_f temperature increases monotonically up to 100 hours, reaching its saturation after 72 hours of aging.

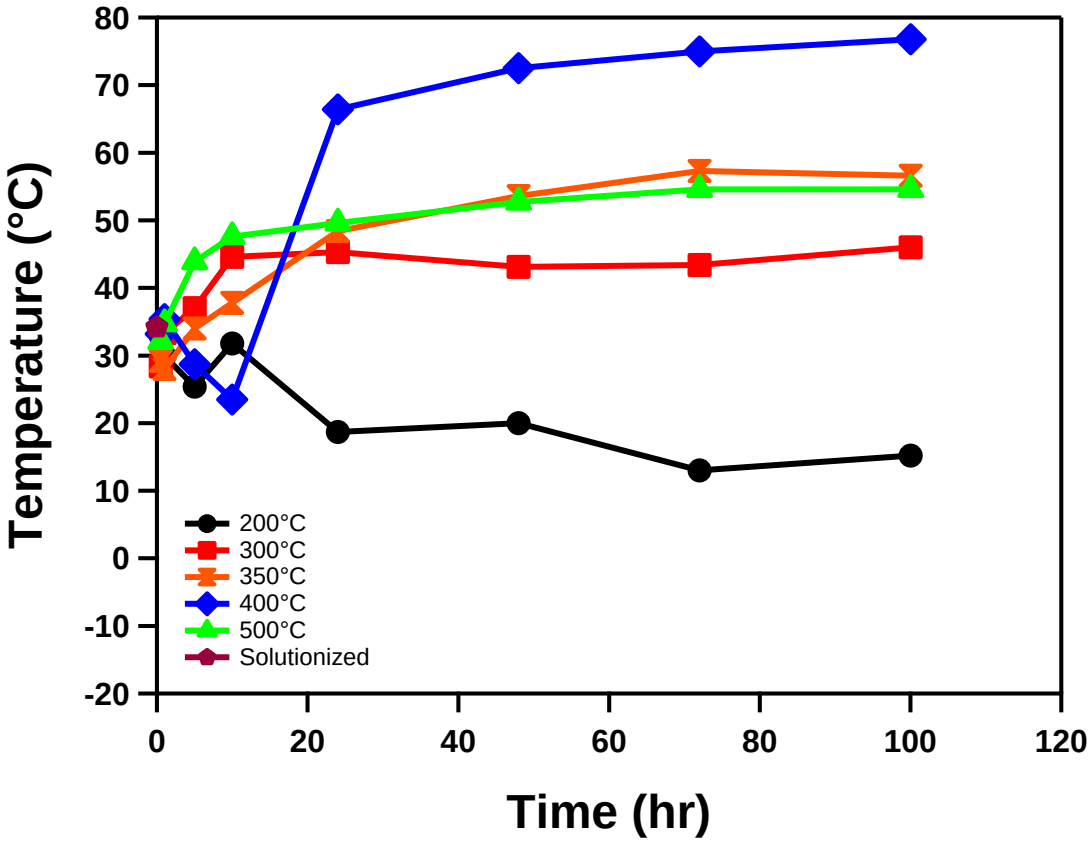

Figure 3.7 A_f temperatures for 50.7 (at%) NiTi after aging

As the aging temperature increases from 200ºC to 300ºC the A_f temperatures also increase. From 300ºC to 350ºC the A_f temperatures are initially higher for 300ºC aging; however, when the heat treatment duration is 24 hours and longer the A_f temperatures are higher for 350ºC aging. During aging at 400ºC the A_f temperatures are initially lower than samples aged at 300ºC, 350ºC, and 500ºC, but higher after 24 hours of aging.

Figure 3.8 shows the A_f temperatures for the 51.2 (at%) NiTi material aged at various temperatures and durations. No transformation is observed for aging at 350ºC below 72 hours, 375ºC below 24 hours, 400ºC below 10 hours, and 450ºC below 0.5 hours. At this composition only increases in A_f with increasing aging temperature are observed. Again, it is important to note that martensitic transformations may occur under the above aging conditions, and it is possible that a decreasing trend exists at low temperatures and short aging durations.

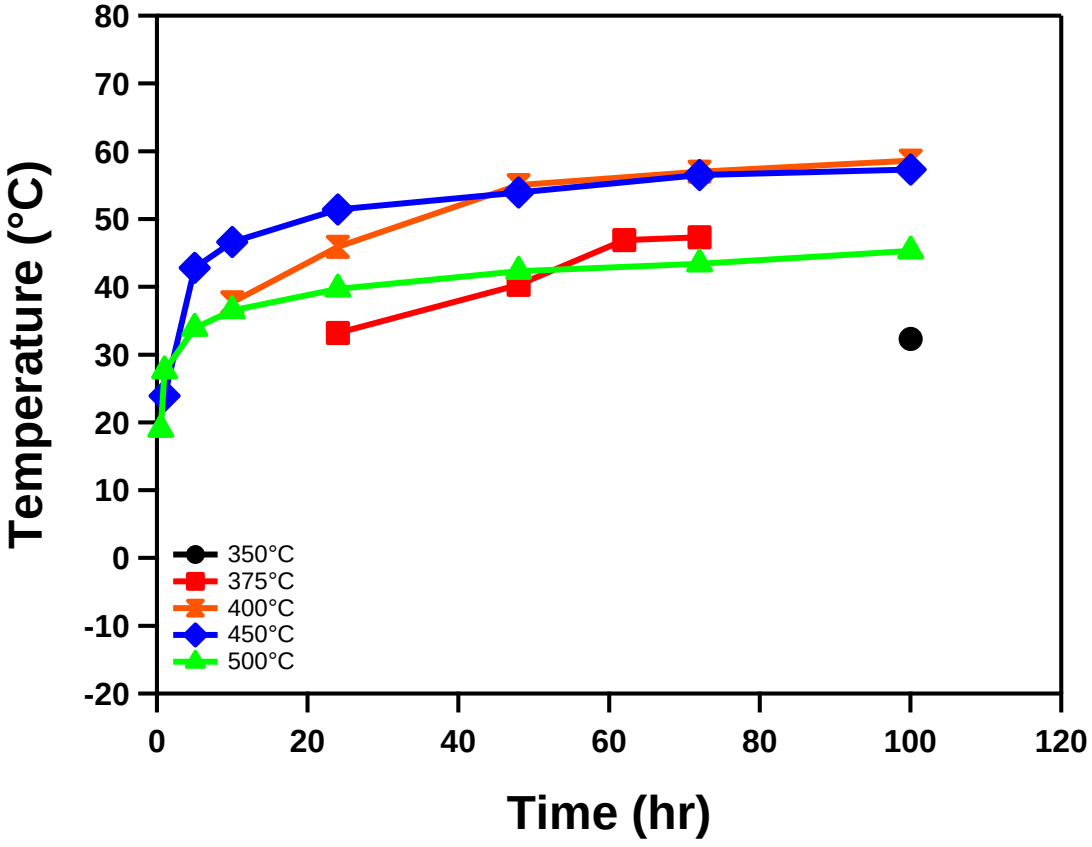

Figure 3.8 A_f temperatures for 51.2 (at%) NiTi after aging

For all aging temperatures the A_f continues to evolve with subsequent aging; no saturation behavior is observed. As the aging temperature increases from 375ºC to 500ºC the concavity of the A_f temperature-aging time curves increases. As the aging temperature increases from 350ºC to 400ºC the A_f temperatures increase as well. From 400ºC to 425ºC the A_f temperatures increase for aging up to 48 hours; for longer aging the difference in A_f temperatures are small. When the aging temperature increases from 450ºC to 500ºC the A_f temperatures decrease. The lowest A_f temperature detected was after aging at 500ºC for 0.5 hours, and the highest A_f temperature detected was after aging at 400ºC for 100 hours.

Figure 3.9 shows the A_f temperatures for the 52.5 (at%) NiTi material aged at various temperatures and durations. No transformation is observed when aging at 375ºC below 48 hours, 400ºC below 5 hours, 425ºC below 1 hour, and 450ºC below 5 hours. At the lowest aging temperature (375ºC) the A_f temperature increases from 48 to 100 hours of aging. After aging at 400ºC the A_f temperature increases up to 10 hours of aging; decreases from 10-24 hours, and then continuously increases from 24-100 hours. When the aging temperature increases to 425ºC there is an increase in A_f temperature from 1-3 hours; from 3 to 48 hours the A_f temperature remains relatively constant, varying by 2ºC; from 48 to 100 hours the A_f temperature increases continuously. When the aging temperature is 450ºC the A_f temperature increases from 5 to 10 hours, remains unchanged from 10-24 hours, and increases continuously from 24-100 hours. At the highest aging temperature (500ºC) the A_f temperature increases monotonically through the entire aging duration.

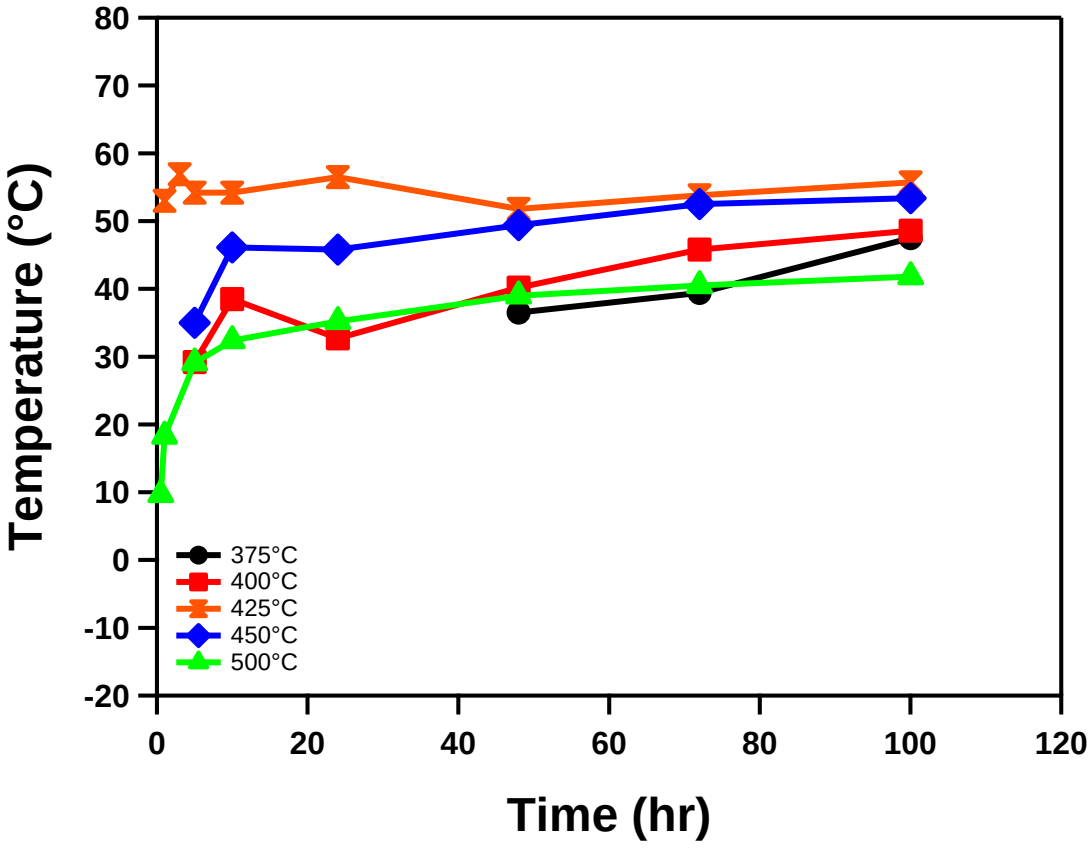

Figure 3.9 A_f temperatures for 52.5 (at%) NiTi after aging

As the aging temperatures increases from 375ºC to 425ºC the A_f temperatures increase as well. When the aging temperature increases from 425ºC to 500ºC the A_f decreases. The highest observed A_f temperature was 56ºC, obtained after aging at 425ºC for 3 hours. The lowest observed A_f temperature was 26ºC, obtained after aging at 500ºC for 0.5 hours.

3.4. Discussion

Two distinct trends are observed in the evolution of the transformation temperatures with subsequent aging. In the first case the transformation temperature decreases initially from the solution treated condition. After sufficient aging the transformation temperature increases. This behavior is observed in the 50.7 (at%) NiTi material after aging at 200ºC and 300ºC. In the second case the transformation temperature increases immediately after the onset of aging, and as the aging duration increases, the transformation temperature begins to saturate. This is observed in all other heat treatments performed on all three NiTi compositions. The lone exception is heat treatments performed at 400ºC on the 50.7 (at%) NiTi material. In this case the transformation temperature decreases initially, but then rapidly increases before approaching saturation. Examples of each of these three trends are shown in Figure 3.10.

The first trend (reduction in transformation temperature) is observed in low temperature aging in the material with the lowest Ni concentration. This agrees with the results of Evirgen [64] and Kim [28] who showed that in low temperature aging the M_s temperature is suppressed. This is attributed to the nucleation of nanoscale precipitates with very short interparticle distances in the matrix. The twinning type changes from type I and II to compound twinning in the areas of the matrix that are constrained between precipitates [16]. The compound twins have a much finer structure in comparison to the type I and II twins found in the single phase condition. The compound twins store more reversible energy and dissipate more energy when martensite nucleates

and grows during the transformation. This increase in reversible and dissipated nucleation energy corresponds to a decrease in M_s [7, 13, 16].

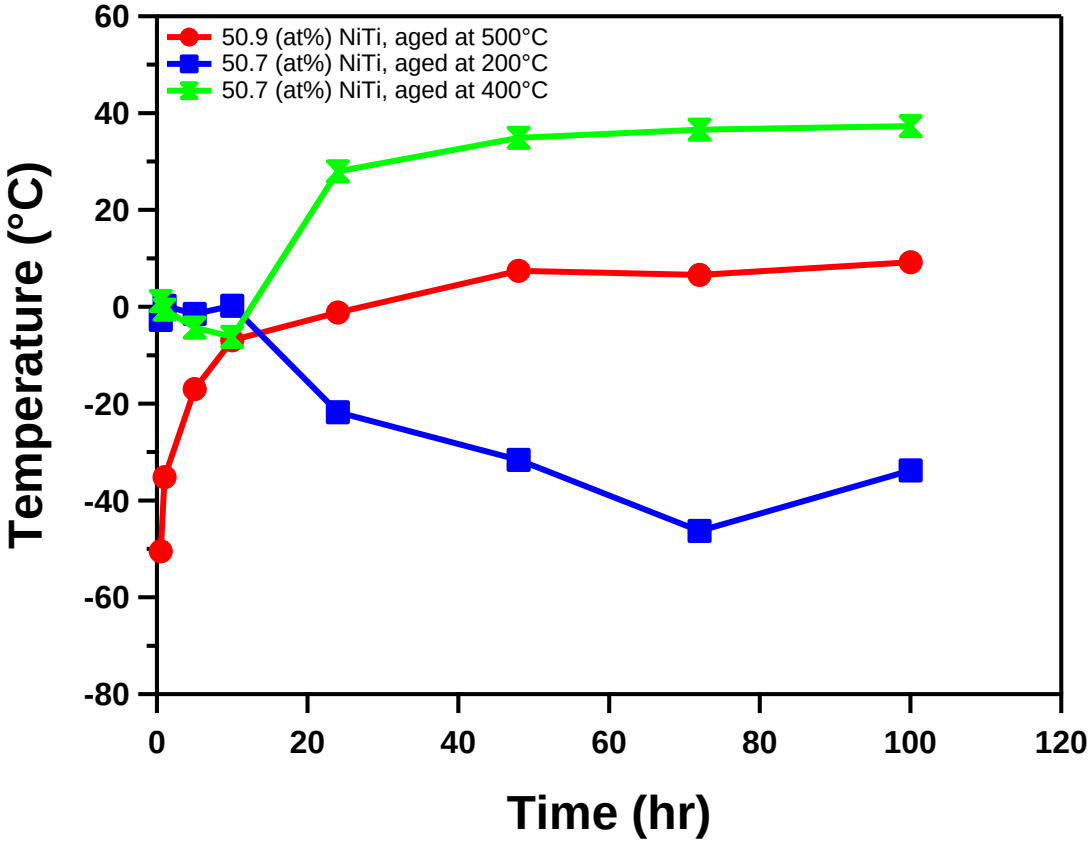

Figure 3.10 Selected M_s temperature-aging time curves showing two different aging trends and anomalous behavior. 50.7 (at%) NiTi aged at 200ºC shows the reduction trend; 50.9 (at%) NiTi aged at 500ºC shows the increasing trend. 50.7 (at%) NiTi aged at 400ºC shows anomalous behavior.

Additionally, if the interparticle distance is smaller than the critical nucleation radius of martensite, then the transformation requires additional driving force to begin [64].

The R_{sr} and A_f temperatures are also reduced by low temperature aging. Figure 3.11 shows the evolution of all three transformation temperatures for the 50.7 (at%) NiTi material during aging at 200ºC.

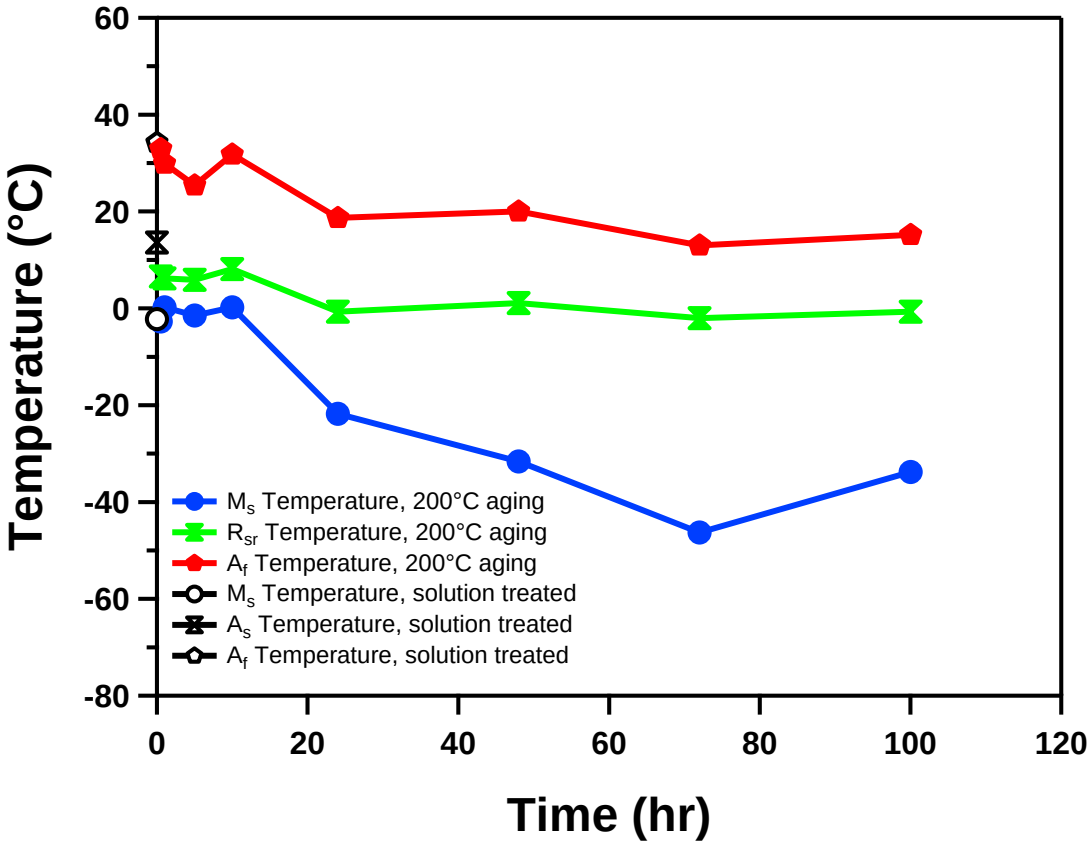

Figure 3.11 M_s, R_{sr}, and A_f temperatures for the 50.7 (at%) NiTi material solution treated and aged at 200ºC. All three transformation temperatures are reduced by low temperature aging.

The M_s temperature is suppressed more than the R_{sr} and A_f temperatures. After 72 hours of aging at 200ºC the M_s temperature decreases by 46ºC, the R_{sr} by 16ºC, and the A_f by 21ºC. Equations (3)-(6) show that the M_s temperature is decreased from T_0 by the presence of reversible and irrecoverable energy. However, the R_{sr} and A_f

temperatures are reduced by reversible energy and elevated by irrecoverable energy. These energy contributions partially counteract each other in the case of the R_{sr} and A_f temperatures, but complement each other in the case of the M_s temperature.

The anomalous behavior of the 50.7 (at%) NiTi material heat treated at 400ºC is explained by the type of transformation that results from this aging condition. In all other heat treatment conditions either a direct B2-B19' transformation or a B2-R-B19' transformation was observed. Figure 3.12 shows the dsc curves for the 50.7 (at%) NiTi material aged at 400ºC; multiple step transformations are observed for durations longer than 30 minutes.

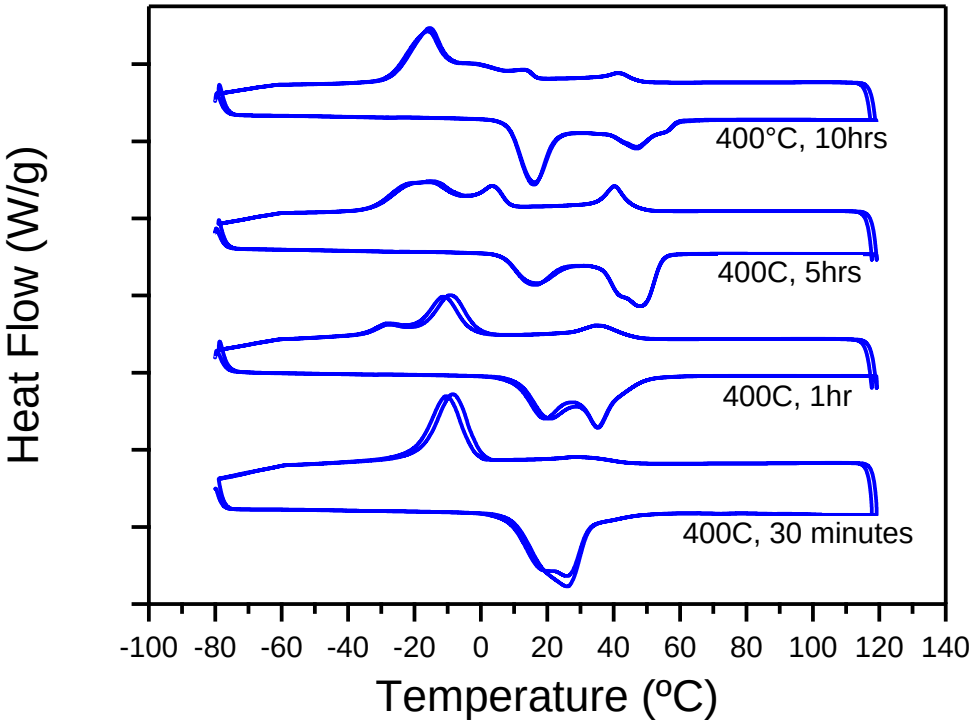

Figure 3.12 Dsc curves for the 50.7 (at%) NiTi material aged from 30 minutes to 10 hours. At 30 minutes the material shows a direct B2-B19' transformation, but for longer durations the distinct multiple step transformation is observed.

Since different regions of the material transform at different temperatures in this case it is difficult to compare the effect of aging at 400ºC in this material to cases where only the B2-B19' and B2-R-B19' transformations occur.

The evolution of the transformation temperatures are attributed mainly to the changes of two factors; these are the composition of the matrix, and the average free distance between precipitates [16, 64]. In the case of aging the 50.7 (at%) NiTi material at 200ºC the transformation temperatures initially decrease due to the reduction in the interparticle distance. As new precipitates form and the number fraction and volume fraction of precipitates increase the interparticle distance decreases as well. However, after 72 hours of aging the trend reverses and the M_s begins to increase. This change in behavior can be explained by the theory of Ostwald ripening. When a second phase nucleates from a solid solution, the surface energy of the dispersed precipitates can be lowered by an increase in their average size. Furthermore, small particles tend to dissolve into the matrix by diffusional processes as large particles continue to grow [68]. As the particles coarsen, the average distance between them increases, decreasing the volume fraction of compound twins that form during the transformation, and reducing their suppressive effect on the martensitic transformation temperature.

At higher aging temperatures and Ni compositions the second trend is observed (the transformation temperatures increase and then saturate). In these cases two scenarios are possible. In one scenario small precipitates with narrow interparticle distances form, reducing the transformation temperatures. However, the timeframe for the formation of these precipitates is extremely short (less than 30 minutes) and they

rapidly coarsen, leading to elevated transformation temperatures. Thus, if the aging temperature is sufficiently short a reduction in transformation temperatures could be observed. In the other scenario, the onset of coarsening occurs concurrently with the formation of nanoscale precipitates, and the interparticle distance begins to increase immediately with precipitate formation; in this case no suppression of transformation temperatures will be observed regardless of aging time.

In heat treatment conditions that exhibit the second trend the transformation temperatures increase above those of the solution treated materials. However, the M_s can only be reduced by energy barriers to martensitic transformation. Thus, if the M_s temperature of an aged NiTi material is higher than that of the solution treated case, it can only be explained by a change in chemical composition. Since the Ni_4Ti_3 precipitates are Ni rich, their formation necessarily depletes the Ni content of the matrix. The T_0 temperature is highly dependent on the Ni content, and as the Ni content of the matrix decreases, the T_0 temperature increases [60].

The evolution of the transformation temperatures is evidently a competition between the effect of interparticle distance and the Ni matrix composition. When the transformation temperatures are suppressed, the interparticle distance is the dominant factor. When the transformation temperatures are elevated, the interparticle distances are large and the change in composition is the dominant factor. This compositional change occurs mostly during nucleation; during the coarsening process the composition change is negligible [69]. Panchenko et. al estimated the Ni concentration in 50.7, 50.8, and 51.0 (at%) NiTi after aging at 400ºC and 500ºC for up to 1.5 hours and showed that the final

matrix concentration was close to 50.5 (at%) Ni in each case. According to the results of Frenzel et. al a compositional change from 50.7 (at%) Ni to 50.5 (at%) increases the M_s by 20ºC, and from 51.0 (at%) Ni to 50.5 (at%) increases the M_s by 80ºC [60].

As the aging temperature increases the transformation temperatures tend to increase until the aging temperature reaches a critical level at which they begin to decrease. For example, in the 50.7 (at%) NiTi material aged at 72 hours the M_s increases from -46ºC to 36ºC when the aging temperature increases from 200ºC to 400ºC. This shift in M_s of 70ºC cannot be explained by a difference in composition since this would require a shift in Ni composition from 50.7 to 49.9 (at%). The increase in transformation temperatures must be then due to a change in interparticle distance. This is supported by the fact that the rate of coarsening increases with temperature [70]. At higher temperatures coarsening occurs more rapidly, and so the precipitates have a larger average size and interparticle distance. When the interparticle distance is large the volume fraction of compound twins decreases (less material is constrained between adjacent precipitates) and less elastic and irrecoverable energy is required to initiate transformation. This corresponds to an increase in transformation temperatures. However, this does not explain why the transformation temperatures decrease when the aging temperature passes the critical point.

In the 50.7 (at%) NiTi material aged at 72 hours, when the aging temperature increases from 400ºC to 500ºC the M_s temperature decreases, and the trend reverses. This decrease in transformation temperatures cannot be attributed to a decrease in interparticle distance, since this would correspond to an increase in thermal hysteresis.

This due to the fact that an increased volume fraction of compound twins must be accompanied by higher reversible and irrecoverable energy barriers. However, this is not the case as show by Figure 3.13.

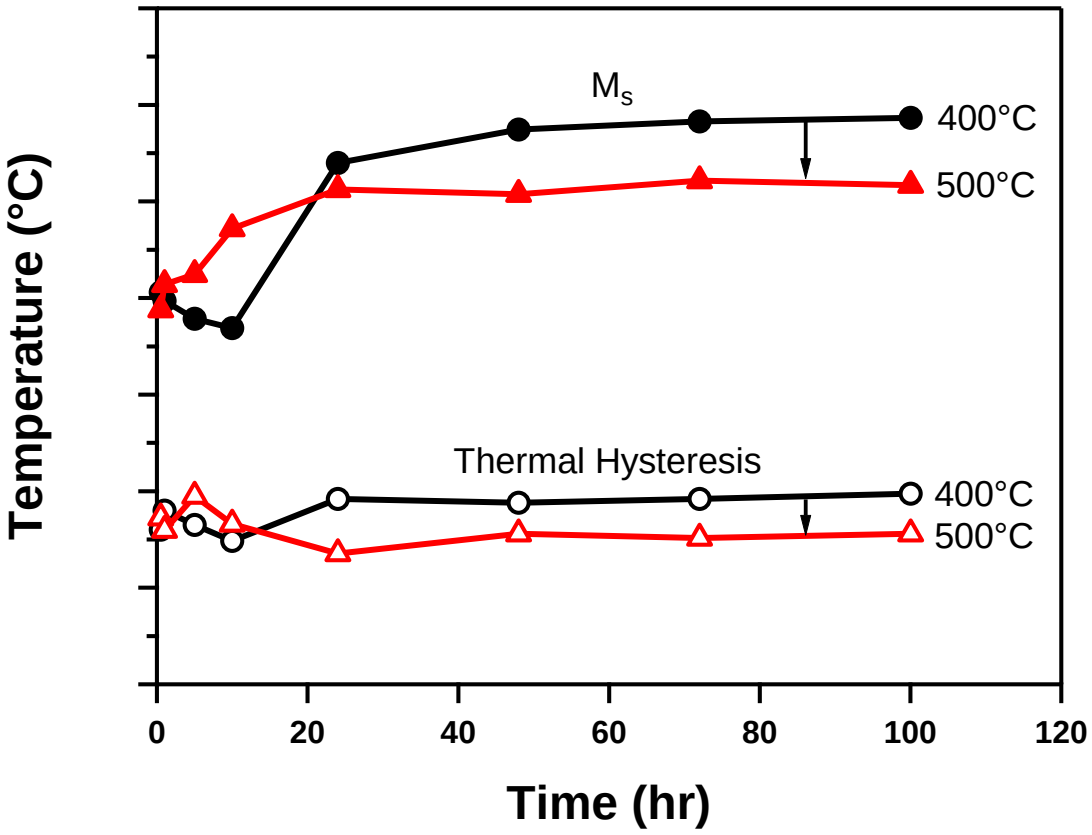

Figure 3.13 M_s temperatures and thermal hysteresis of a 50.7 (at%) NiTi material aged at 400ºC and 500ºC.

The figure shows the evolution of the transformation temperatures after the critical aging temperature; from 400ºC to 500ºC the M_s decreases. However, the hysteresis decreases as well. The reversal in trend can instead be explained by the variation of the nucleation rate with temperature.

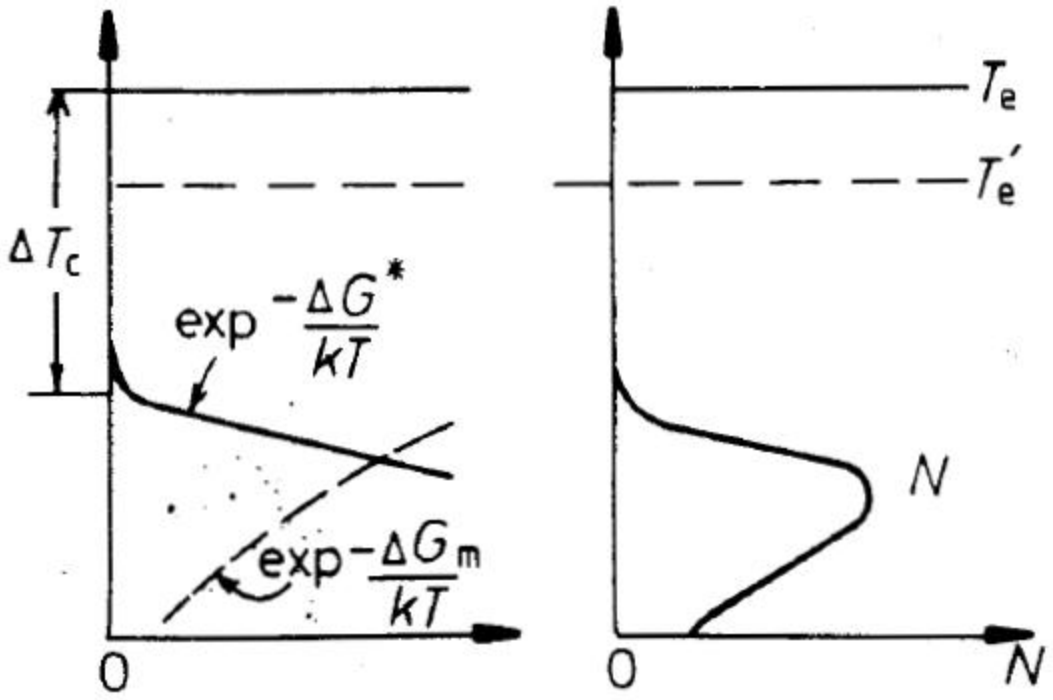

Figure 3.14 Left: variation of activation energy of atomic migration and driving force for nucleation with temperature. Right: variation of nucleation rate with temperature [71].

Figure 3.14 shows that initially the nucleation rate increases with increasing temperature due to the increasing ease of atomic motion (dashed line, left figure). However, as the temperature continues to increase the driving force for nucleation decreases (solid line, left figure) which leads to a drop in nucleation rate. Since the coarsening rate continuously increases with aging temperature but the nucleation rate decreases at the critical point, the volume fraction of precipitates decreases. Since the volume fraction of precipitates is lower, the interparticle distances are larger, and the Ni composition is higher.

As the aging temperature increases the concavity of the aging temperature-transformation temperature curves increases with it. This means that at higher temperatures the transformation temperatures evolve more rapidly and reach their saturation values more quickly. At high temperatures the rate of coarsening increases due to the increased rate of diffusion.

The transformation temperatures are lower in the materials with higher Ni content than in the 50.7 (at%) NiTi composition.

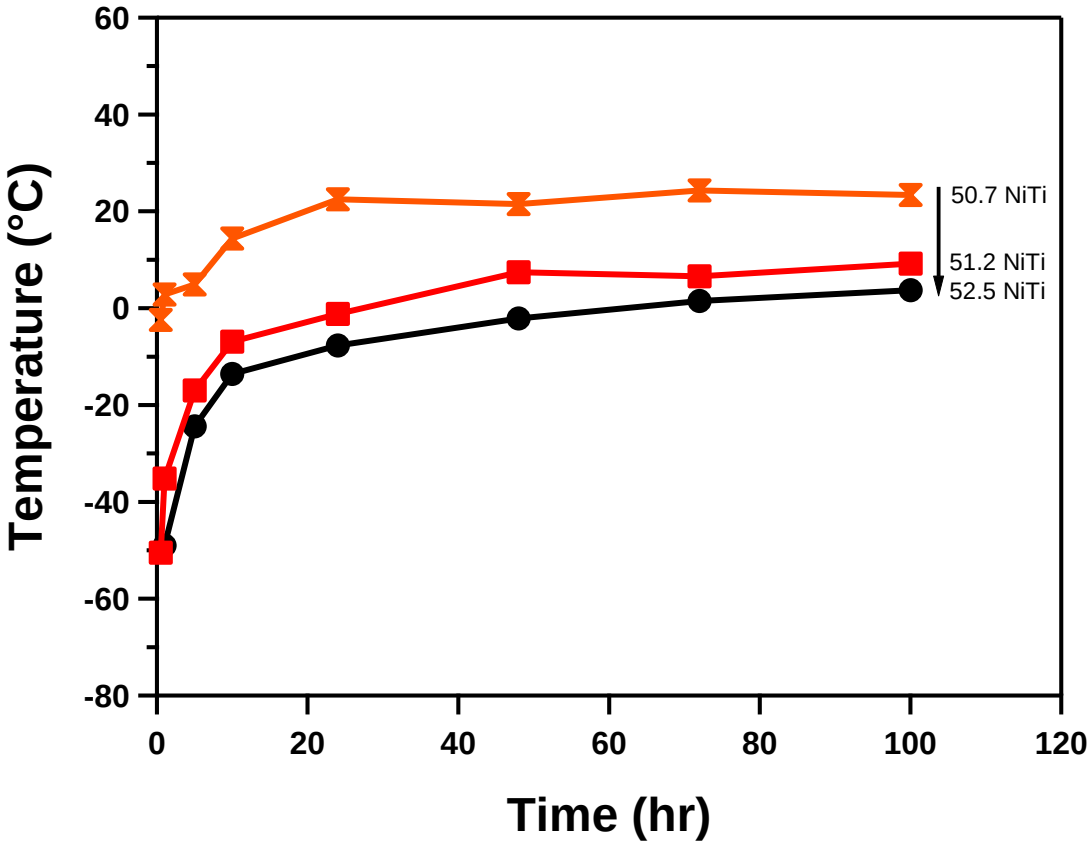

Figure 3.15 M_s temperatures for aging at 500ºC in all three Ni compositions. As the initial Ni concentration increases, the M_s temperature decreases.

Figure 3.15 shows the M_s temperature for all three Ni compositions aged at 500ºC. As the initial Ni concentration increases the M_s temperatures decrease. When the initial supersaturation of Ni is higher the volume fraction of precipitates formed increases [16, 69]. When the volume fraction of precipitates is higher, the interparticle distances are smaller, which causes a larger volume fraction of compound twins to form. The higher volume fraction of compound twins further suppresses the transformation temperatures.

\

4. EFFECT OF AGING ON HYSTERESIS

4.1. Results

Figure 4.1 shows the thermal hysteresis for the 50.7 (at%) NiTi material. At the lowest aging temperature (200ºC) the hysteresis decreases up to 5 hours of aging, increases from 5 to 72 hours, and then decreases from 72 to 100 hours. When the aging temperature increases to 300ºC the hysteresis decreases up to 1 hour of aging, decreases from 1 to 72 hours, and then decreases slightly from 72 to 100 hours. After elevating the heat treatment temperature to 400ºC the hysteresis decreases up to 10 hours of aging, increases from 10 to 24 hours of aging, and then remains relatively constant from 24 to 100 hours of aging. At the highest aging temperature (500ºC) the hysteresis increases from 1 to 5 hours of aging, decreases from 5 to 24 hours, increases from 24 to 48 hours, and then remains relatively constant from 48 to 100 hours.

At aging temperatures above 300ºC the thermal hysteresis exhibits saturation behavior. During aging at 350ºC and 400ºC the hysteresis saturates after 24 hours of aging; at 500ºC the hysteresis saturates after 48 hours of aging. During aging at 200ºC and 300ºC the hysteresis continues to evolve up to and including 100 hours.

When the aging temperature increases from 300ºC to 350ºC the hysteresis decreases; from 350ºC to 400ºC there is little change in the hysteresis; from 400ºC to 500ºC the hysteresis is higher initially from 0.5 to 10 hours, but lower from 10 to 100 hours.

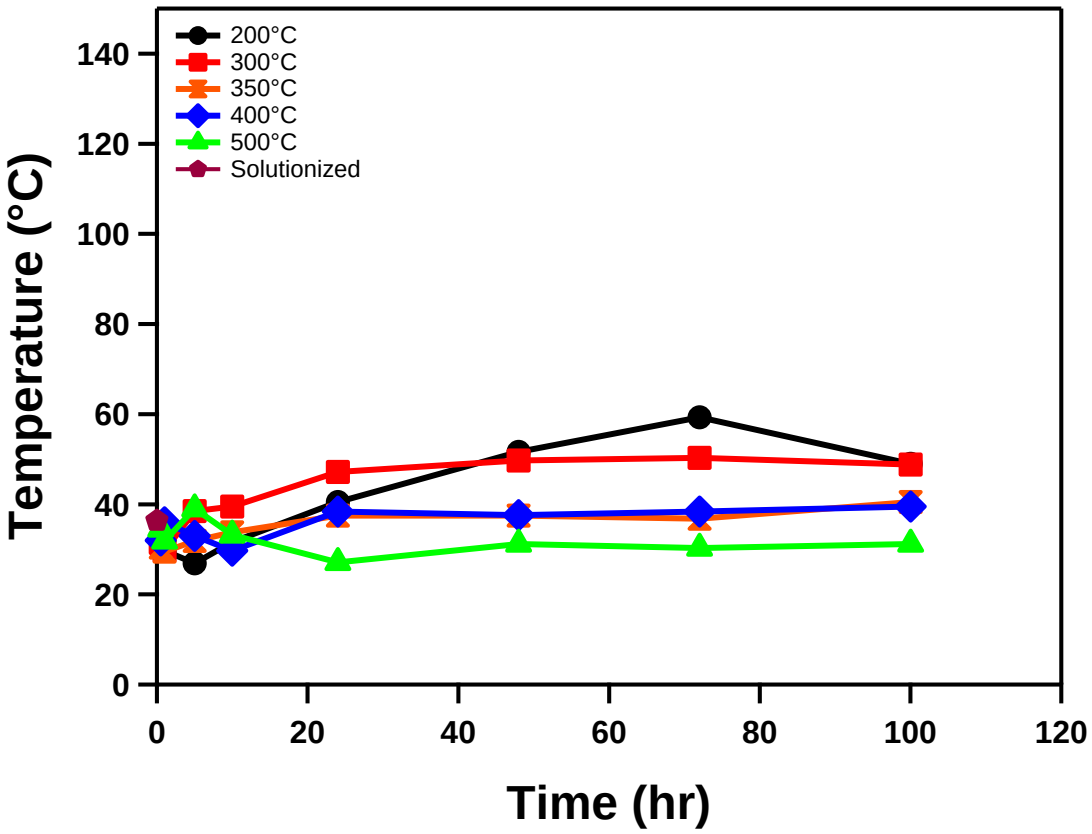

Figure 4.1 Thermal hysteresis for 50.7 (at%) NiTi after aging

The highest hysteresis (59ºC) was observed after aging at 200ºC for 72 hours, and the lowest (25ºC) was observed after aging at 200ºC for 5 hours. In several cases the hysteresis of the aged treated materials was lower than that of the solution treated sample.

Figure 4.2 shows the thermal hysteresis for the 51.2 (at%) NiTi material. With the exception of aging at 375ºC from 48 to 72 hours the hysteresis decreases with increasing aging time. Again, due to the lower temperature limit of the DSC equipment

(-80ºC) it is possible that increases in hysteresis occur under low duration, low temperature aging treatments, but cannot be observed.

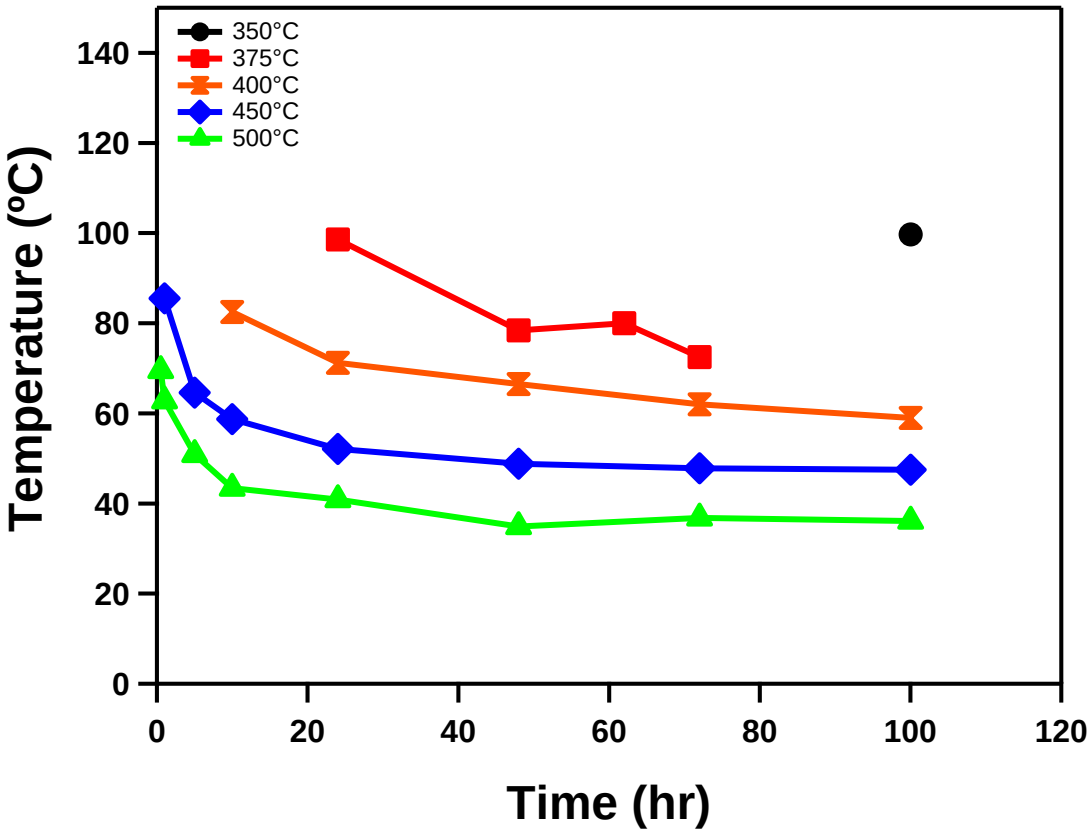

Figure 4.2 Thermal hysteresis for 51.2 (at%) NiTi after aging

As the aging temperature increases the thermal hysteresis decreases. Additionally, as the aging temperature increases the concavity of the hysteresis-aging time curves increases as well. Finally, while the hysteresis continues to evolve up to 100 hours during aging at 400ºC, saturation behavior is observed during aging at 450ºC and 500ºC.

The highest hysteresis observed (100ºC) was obtained after aging at 350ºC for 100 hours, while the lowest (35ºC) was obtained after aging at 500ºC for 48 hours.

Figure 4.3 shows the thermal hysteresis for the 52.2 (at%) NiTi material. After aging at 375ºC, 400ºC, and 500ºC, only decreases in hysteresis are observed. During aging at 425ºC slight increases in hysteresis are observed from 0.5 to 1 hour of aging, and from 10 to 24 hours of aging. An increase in hysteresis is also observed during aging at 450ºC from 5 to 10 hours.

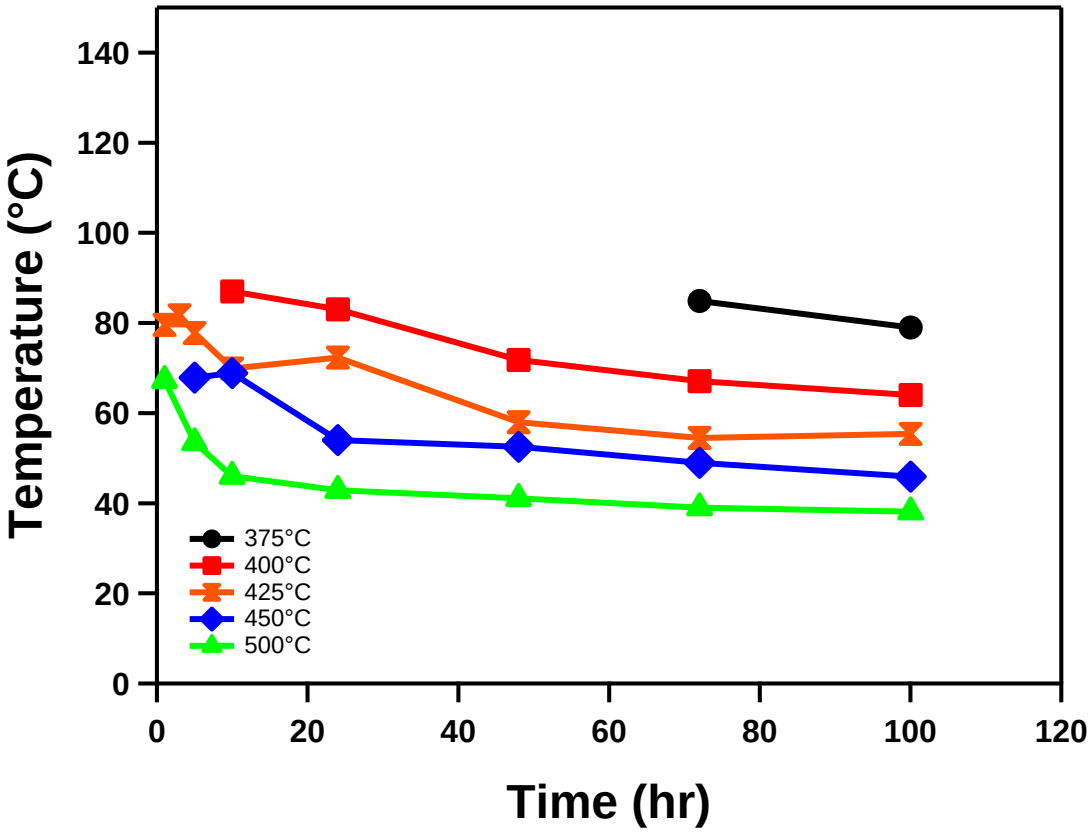

Figure 4.3 Thermal hysteresis for 52.5 (at%) NiTi after aging

The thermal hysteresis behavior during aging in this material composition is similar to the 51.2 (at%) NiTi material. As the aging temperature increases, the thermal hysteresis decreases. The concavity of the hysteresis-aging time curves also increases with aging temperature. However, no saturation behavior is observed and the hysteresis continues to evolve with aging time even at 500ºC.

The highest observed thermal hysteresis was 87ºC, obtained after aging at 400ºC for 10 hours. The lowest observed thermal hysteresis was 38ºC, obtained after aging at 500ºC for 100 hours.

4.2. Discussion

As the aging temperature increases, the thermal hysteresis decreases. There is a single exception to this trend; in the 50.7 (at%) NiTi material aged at 200ºC the hysteresis is lower until 48 hours of aging. Further aging at this temperature yields higher thermal hysteresis than at higher aging temperatures.

The rate of coarsening of precipitates increases with temperature [70]. At low aging temperatures the precipitates are small and packed closely together. This has several important consequences for the thermal hysteresis. The thermal hysteresis depends on the resistance of the matrix to interfacial motion and defect generation [5, 7, 10, 11]. When the interparticle distance is small there is a higher density and volume fraction of compound twins [16]. This corresponds to a higher surface area of interacting martensite-martensite interfaces. Additionally, when the precipitates are coherent with the matrix there is an elastic strain field surrounding each particle; this elastic strain field

serves as a preferential nucleation site for martensite. When the number of precipitates increases it follows that a larger number of variants and martensite-martensite interfaces form. When the number of interacting martensite-martensite interfaces increases the density of frictional energy expended during transformation also increases. Small precipitates also strengthen the matrix against interfacial motion which increases the thermal hysteresis [16]. After coarsening the precipitates become large and no longer effectively strengthen the matrix [67].

The evolution of the thermal hysteresis with respect to aging time differs between the low (50.7 at% NiTi) and high (51.2, 52.5 at% NiTi) Ni content materials. When the Ni content is low the thermal hysteresis reaches its saturation relatively quickly (24-48 hours), except during aging at 200ºC where slow kinetics delays the saturation behavior. In the higher Ni content materials the hysteresis continues to evolve even up to 72-100 hours. This is likely due to the difference in the volume fraction of precipitates. When the initial Ni content is low, the volume fraction of precipitates formed is also low [16]. In this case less time is required for the precipitate structure to reach an equilibrium state.

Figure 4.4 shows the evolution of the thermal hysteresis for all three NiTi compositions during aging at 500ºC. As the initial Ni content increases the thermal hysteresis after aging increases as well. When the initial supersaturation is higher, the volume fraction of precipitates formed during aging increases [69]. The higher volume fraction of precipitates corresponds to a decrease in interparticle distance, which increases the frictional energy dissipated during transformation.

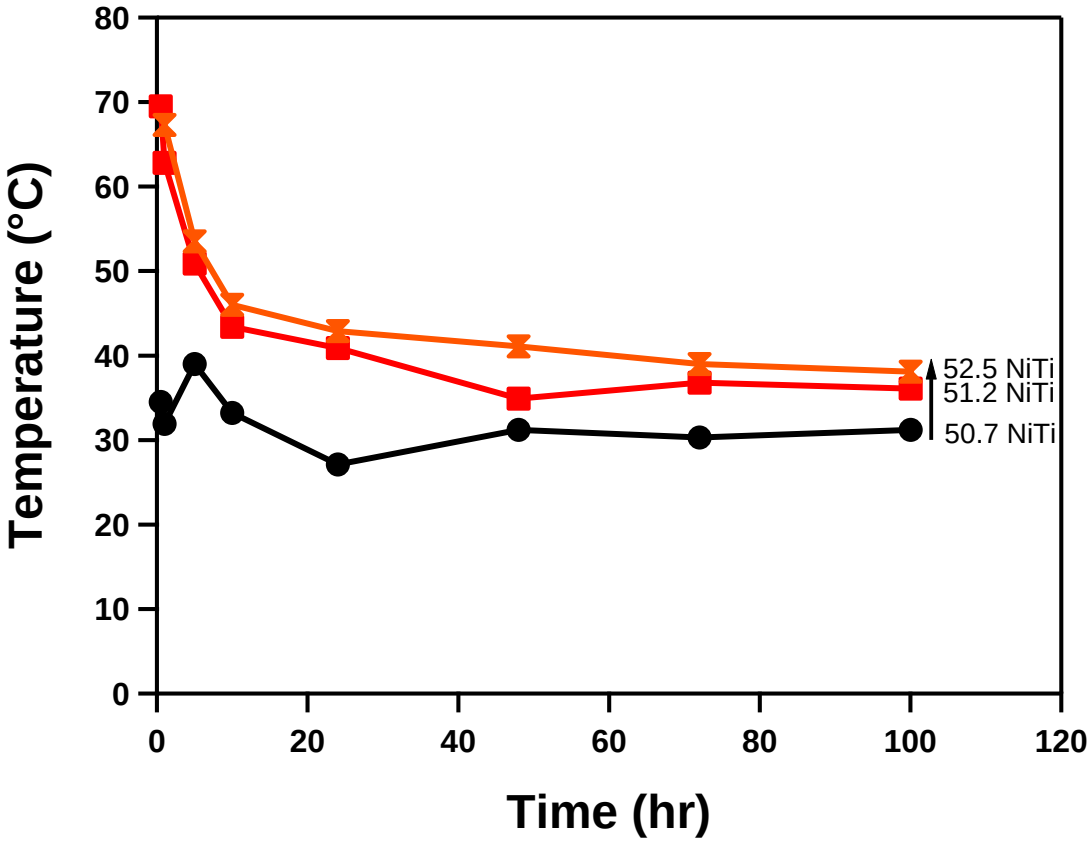

Figure 4.4 Thermal hysteresis for all three NiTi compositions aged at 500ºC.

In the 50.7 (at%) NiTi material the thermal hysteresis can be suppressed below the solution treated case. This has been attributed to a reduction in matrix strength after precipitate formation [66]. After coarsening, the precipitates are large and incoherent; in this case they are less effective at resisting interfacial motion. Additionally, the reduction in Ni content reduces the effectiveness of solid solution strengthening. So, in cases where the volume fraction of precipitates is small, and the average particle distance is

large, then the reduction in matrix strength can reduce the thermal hysteresis from the solution treated condition.

For applications requiring shape memory alloys, the engineering specifications will include the M_s temperature and the thermal hysteresis. The relevant data collected in this work is summarized in Figure 4.5. The figure shows the obtainable thermal hysteresis/M_s temperature combinations.

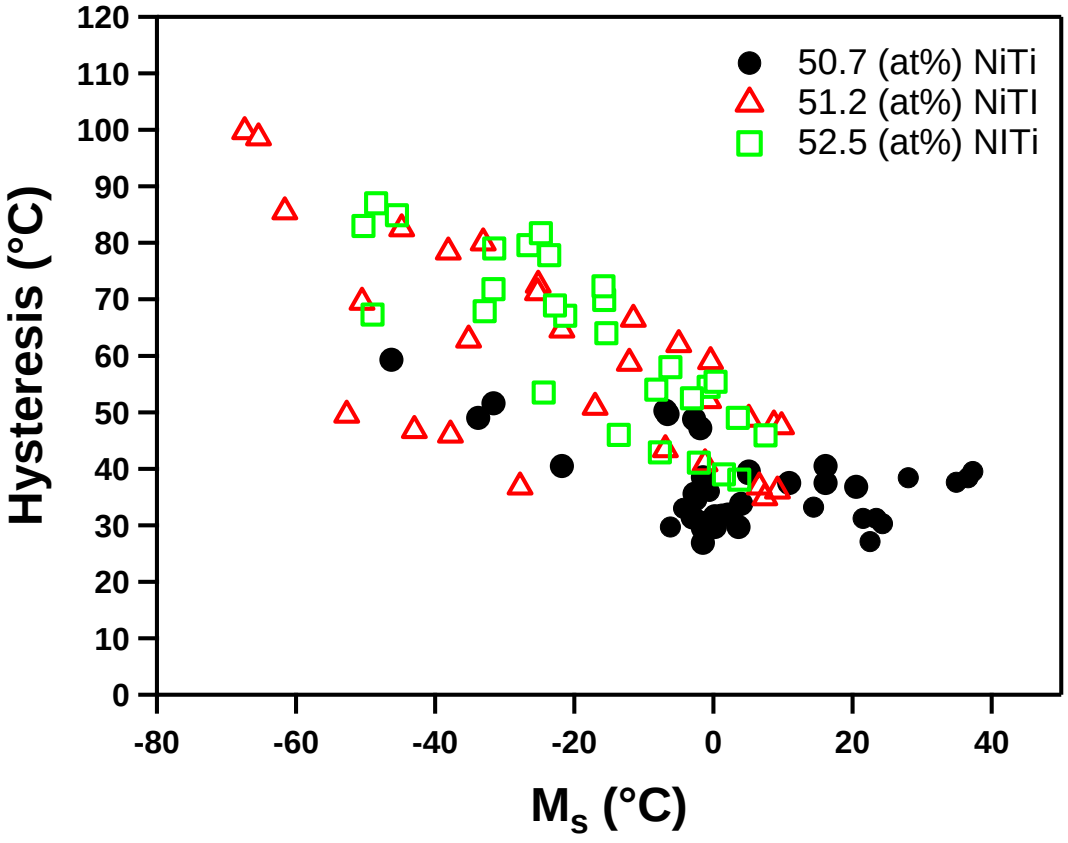

Figure 4.5 The thermal hysteresis and M_s temperature for every heat treatment investigated in this work. This figure summarizes the obtainable thermal hysteresis/M_s temperature combinations.

It should be noted that some of the boundaries of the data in the figure are in part determined by the limitations of the DSC equipment, in particular the upper left portion of the figure. However, some general trends in the obtainable thermal hysteresis/M_s temperatures can be observed. High M_s temperatures come at the cost of low thermal hysteresis. High thermal hysteresis can only be obtained when the M_s temperatures are low. The upper limit of the M_s temperatures in the 50.7 (at%) NiTi material is 37ºC, but the limit of the higher Ni content materials is about 10ºC. In contrast the lower limit of the high Ni content materials is so low that it cannot be observed, but for the 50.7 (at%) NiTi material this limit is -47ºC.

By varying the composition and the heat treatment conditions a wide variety of combinations are possible. For example, with a fixed hysteresis of 50ºC materials with an M_s temperature between -57ºC and 10ºC can be produced. Materials with a fixed M_s temperature of -20ºC can be produced with a thermal hysteresis between 40ºC and 80ºC.

3-D data analysis can be used to select the correct combination of composition, aging time, and aging temperature to obtain the desired combination of M_s temperature and thermal hysteresis. In the M_s temperature-aging temperature-aging time space, the data from each individual Ni composition forms a surface. Interpolation could be used to predict the M_s temperature and thermal hysteresis of the data points between the surfaces, forming a solid volume. The surface plots for all three materials are shown in Figure **4.6**.

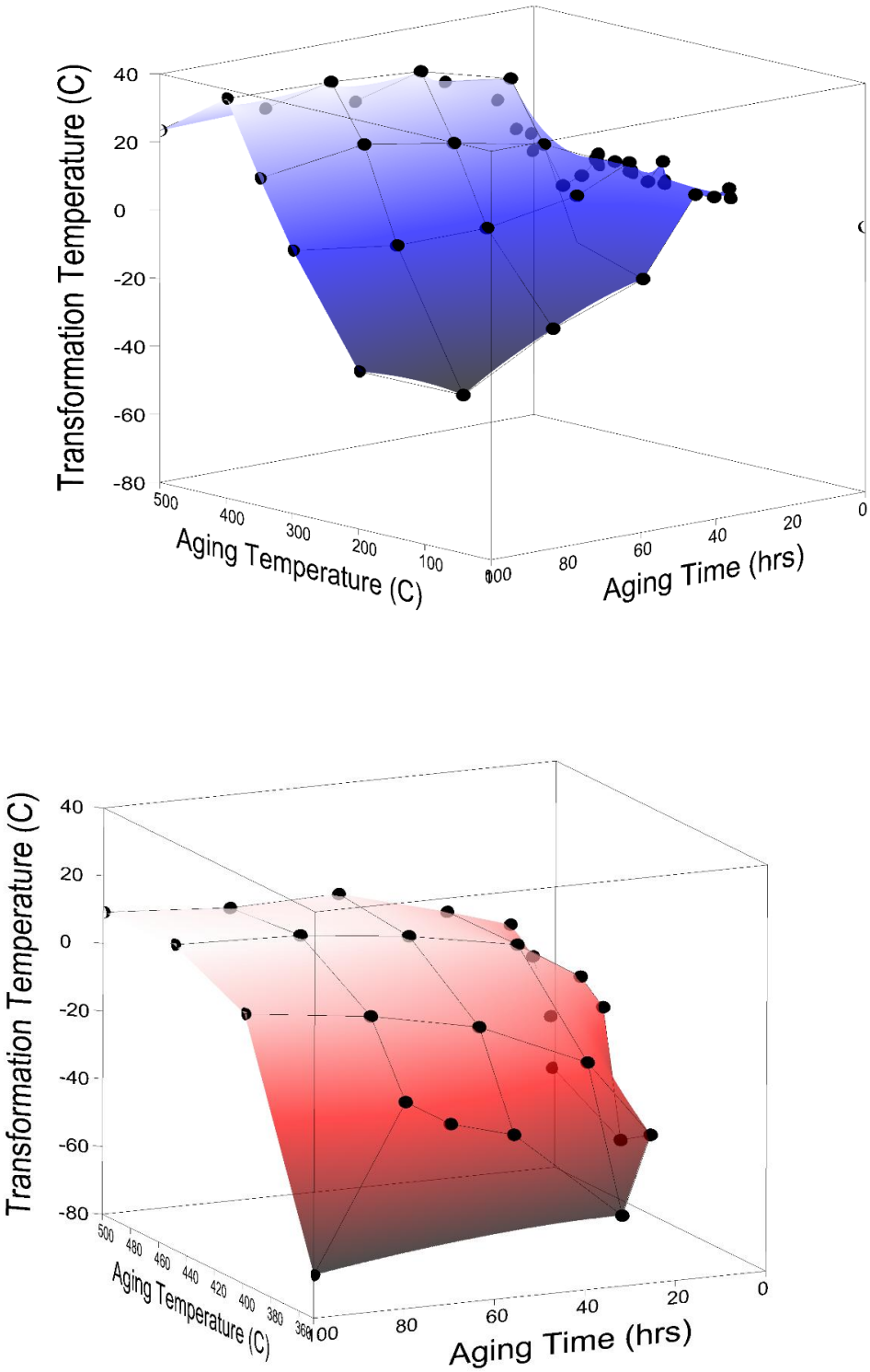

Figure 4.6 M_s temperature-aging temperature-aging time 3d surfaces for all three NiTi compositions. a) 50.7 (at%) NiTi, b) 51.2 (at%) NiTi, c) 52.5 (at%) NiTi

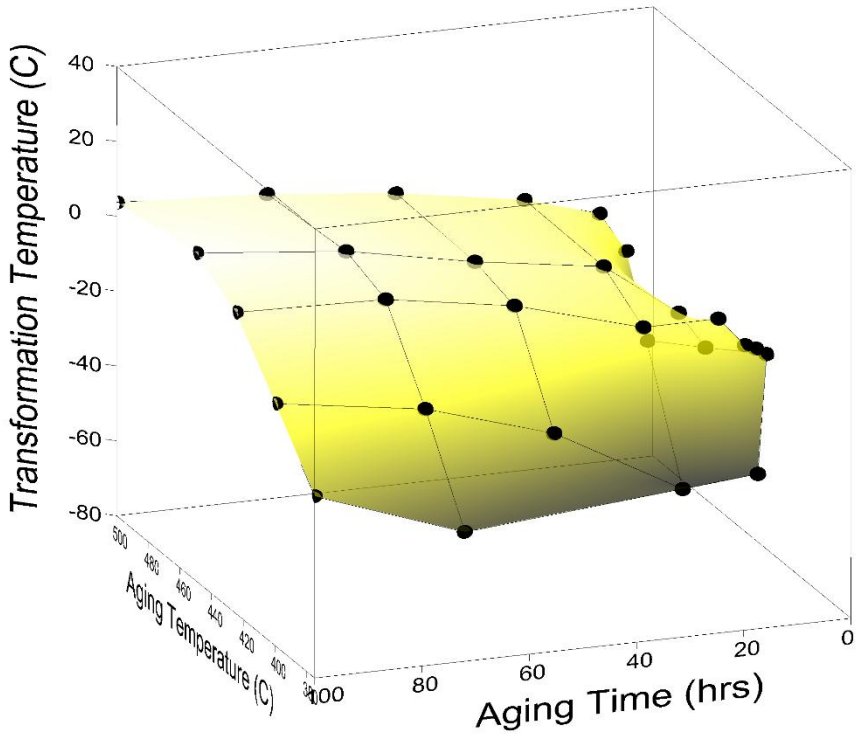

Figure 4.6 Continued

5. CONCLUSION

5.1. Conclusion

Binary NiTi materials of three different, Ni rich compositions were solution treated to obtain a single phase microstructure. Each material was then systematically subjected to aging treatments under different temperatures and durations. The transformation behavior in each condition were measured using DSC to determine the effect of aging on the transformation temperatures and thermal hysteresis under stress free conditions.

The effect of aging on the transformation behavior in the 50.7 (at%) NiTi material was very complex. At low aging temperatures the transformation temperatures were suppressed; at higher aging temperatures they increased. The transformation temperatures increased with increasing aging temperature. At low aging temperatures the transformation temperatures decreased initially; but after long duration aging began to increase. At higher aging temperatures the transformation temperatures increased monotonically with aging duration.

In the higher Ni concentration materials (51.2 and 52.5 at%) the transformation temperatures were highly suppressed after only 30 minutes of aging. Further aging increased the transformation temperatures monotonically with increasing aging time. As the initial Ni content increased the transformation temperatures decreased.

The thermal hysteresis decreased as the aging temperature increased. In the 50.7 (at%) NiTi material the hysteresis saturated after 48-72 hours of aging. In the 51.2 and 52.5 (at%) NiTi materials the thermal hysteresis continued to evolve up to 100 hours of aging. As the initial Ni concentration increased the thermal hysteresis increased as well.

Materials with high M_s temperatures of up to 37ºC were obtainable, but were accompanied by low thermal hysteresis. The opposite was also true, as materials with high thermal hysteresis of up to 100ºC were accompanied by very low M_s temperatures. High temperature, low hysteresis materials were obtained by using a material with a low initial supersaturation of Ni, while low temperature, high hysteresis materials were obtained by using high initial Ni content materials.

5.2. Future studies

In this work the effects of aging on the transformation temperatures and hysteresis were described in terms of the matrix composition, precipitate size, precipitate volume fraction, and interparticle spacing. These factors should be quantified using microscopic characterization techniques to further understand the relative importance of each effect, and at which points in the aging curve they come into play.

While the effects of aging temperature and supersaturation on the rate of coarsening and nucleation are understood in general terms, quantification of how these mechanisms are affected by the heat treatment conditions would allow predictions of the transformation temperatures and thermal hysteresis.

Further studies should be performed on materials with Ni contents between 50.7 (at%) and 51.2 (at%) to further populate the M_s temperature and thermal hysteresis plots.

This work does not address the stress dependence of the thermal hysteresis; the behavior of aged treated Ni-rich materials under mechanical loading will be important for designing microstructures for engineering applications.

Finally, the effect of these aging treatments on the failure behavior, fatigue behavior, and mechanical properties of these materials should be characterized.

REFERENCES

[1] Chang LC, Read TA. T Am I Min Met Eng 1951;191:47.

[2] Otsuka K, Ren X. Prog Mater Sci 2005;50:511.

[3] tsuka , Wayman CM. Shape memory materials. Cambridge ; New York: Cambridge University Press, 1998.

[4] Funakubo H. Shape memory alloys. New York: Gordon and Breach Science Publishers, 1987.

[5] Ortin J, Planes A. Acta Metall Mater 1988;36:1873.

[6] Planes A, Macqueron JL, Ortin J. Phil Mag Lett 1988;57:291.

[7] Olson GB, Cohen M. Scripta Metall Mater 1975;9:1247.

[8] Ahlers M. Philos Mag A 2002;82:1093.

[9] Raghavan V, Cohen M. Acta Metall Mater 1972;20:779.

[10] Olson GB, Cohen M. Scripta Metall Mater 1977;11:345.

[11] Van Humbeeck J, Aernoudt E, Delaey L, Li L, Verguts H, Ortin J. Revue de physique appliquée 1988;23:557.

[12] Liu YN. Thermodynamic analysis of thermoelastic martensitic transformations. In: Kang SG, Kobayashi T, editors. Designing, Processing and Properties of Advanced Engineering Materials, Pts 1 and 2, vol. 449-4. Stafa-Zurich: Trans Tech Publications Ltd, 2004. p.1325.

[13] Salzbrenner RJ, Cohen M. Acta Metall Mater 1979;27:739.

[14] Ortin J, Planes A. Acta Metall Mater 1989;37:1433.

[15] Daroczi L, Beke DL, Lexcellent C, Mertinger V. Scripta Mater 2000;43:691.

[16] Panchenko EY, Chumlyakov YI, Kireeva IV, Ovsyannikov AV, Sehitoglu H, Karaman I, Maier YHJ. Phys Met Metallogr+ 2008;106:577.

[17] Palanki Z, Daroczi L, Lexcellent C, Beke DL. Acta Mater 2007;55:1823.

[18] Bhattacharya K. Microstructure of martensite : why it forms and how it gives rise to the shape-memory effect. Oxford ; New York: Oxford University Press, 2003.

[19] Sehitoglu H, Hamilton R, Canadinc D, Zhang XY, Gall K, Karaman I, Chumlyakov Y, Maier HJ. Metall Mater Trans A 2003;34:5.

[20] Kumar PK, Lagoudas DC. Introduction to Shape Memory Alloys. Shape Memory Alloys, vol. 1. Springer US, 2008. p.1.

[21] Otsuka K, Kakeshita T. Mrs Bull 2002;27:91.

[22] Zhang XY, Sehitoglu H. Mat Sci Eng a-Struct 2004;374:292.

[23] Allafi JK, Dlouhy A, Neuking K, Eggeler G. J Phys Iv 2001;11:529.

[24] Kim JI, Miyazaki S. Metall Mater Trans A 2005;36A:3301.

[25] Liu YN, Chen X, McCormick PG. J Mater Sci 1997;32:5979.

[26] Zheng YF, Jiang F, Li L, Yang H, Liu YN. Acta Mater 2008;56:736.

[27] Gall K, Sehitoglu H, Chumlyakov YI, Kireeva IV, Maier HJ. J Eng Mater-T Asme 1999;121:28.

[28] Kim JI, Liu YN, Miyazaki S. Acta Mater 2004;52:487.

[29] Peltonen M, Lindroos T, Kallio M. J Alloy Compd 2008;460:237.

[30] Allafi JK, Dlouhy A, Eggeler G. J Phys Iv 2003;112:681.

[31] Eggeler GF, Neuking K, Dlouhy A, Kobus E. Shape Memory Materials 2000;327-3:183.

[32] Bataillard L, Bidaux JE, Gotthard R. Philos Mag A 1998;78:327.

[33] Carroll MC, Somsen C, Eggeler G. Scripta Mater 2004;50:187.

[34] Dlouhy A, Bojda O, Somsen C, Eggeler G. Mat Sci Eng a-Struct 2008;481:409.

[35] Dlouhy A, Khalil-Allafi J, Eggeler G. Philos Mag 2003;83:339.

[36] Eggeler G, Allafi JK, Dlouhy A, Ren X. J Phys Iv 2003;112:673.

[37] Fan GL, Chen W, Yang S, Zhu JH, Ren XB, Otsuka K. Acta Mater 2004;52:4351.

[38] Johnson AJW, Hamilton RF, Sehitoglu H, Biallas G, Maier HJ, Chumlyakov YI, Woo HS. Metall Mater Trans A 2005;36A:919.

[39] Khalil-Allafi J, Eggeler G, Schmahl WW, Sheptyakov D. Mat Sci Eng a-Struct 2006;438:593.

[40] Sitepu H, Schmahl WW, Eggeler G, Allafi JK, Tobbens DM. J Phys Iv 2003;112:643.

[41] Chumlyakov YI, Efimenko SP, Kireeva IV, Panchenko EY, Sehitogly H, Gall K, Yahia LH. Dokl Phys 2001;46:849.

[42] Jiang F, Liu YN, Yang H, Li L, Zheng YF. Acta Mater 2009;57:4773.

[43] Sehitoglu H, Jun J, Zhang X, Karaman I, Chumlyakov Y, Maier HJ, Gall K. Acta Mater 2001;49:3609.

[44] Gall K, Yang N, Sehitoglu H, Chumlyakov YI. Int J Fracture 2001;109:189.

[45] Eggeler G, Hornbogen E, Yawny A, Heckmann A, Wagner M. Mat Sci Eng a-Struct 2004;378:24.

[46] Wagner MFX, Dey SR, Gugel H, Frenzel J, Somsen C, Eggeler G. Intermetallics 2010;18:1172.

[47] Miyazaki S, Wayman CM. Acta Metall Mater 1988;36:181.

[48] Liu Y, Mccormick PG. Acta Metall. Mater. 1994;42:2401.

[49] Cesari E, Pons J, Santamarta R, Segui C, Stroz D, Morawiec H. Applied Crystallography 2001:171.

[50] Nishida M, Ishiuchi K, Fujishima K, Hara T. Mater Trans 2006;47:645.

[51] Stroz D. J Phys Iv 2003;112:689.

[52] Wang XB, Li K, Schryvers D, Verlinden B, Van Humbeeck J. Scripta Mater 2014;72-73:21.

[53] Zhou Y, Fan G, Zhang J, Ding X, Ren X, Sun J, Otsuka K. Mat Sci Eng a-Struct 2006;438:602.

[54] Zhou YM, Zhang J, Fan GL, Ding XD, Sun J, Ren XB, Ostsuka K. Acta Mater 2005;53:5365.

[55] Allafi JK, Ren X, Eggeler G. Acta Mater 2002;50:793.

[56] Tirry W, Schryvers D. Acta Mater 2005;53:1041.

[57] Fujishima K, Nishida M, Morizono Y, Yamaguchi K, Ishiuchi K, Yamamuro T. Mat Sci Eng a-Struct 2006;438:489.

[58] Khalil-Allafi J, Dlouhy A, Eggeler G. Acta Mater 2002;50:4255.

[59] Tang W, Sundman B, Sandstrom R, Qiu C. Acta Mater 1999;47:3457.

[60] Frenzel J, George EP, Dlouhy A, Somsen C, Wagner MFX, Eggeler G. Acta Mater 2010;58:3444.

[61] Ball JM, James RD. Philos T Roy Soc A 1992;338:389.

[62] Cui J, Chu YS, Famodu OO, Furuya Y, Hattrick-Simpers J, James RD, Ludwig A, Thienhaus S, Wuttig M, Zhang ZY, Takeuchi I. Nat Mater 2006;5:286.

[63] Chumlyakov YI, Kireeva IV, Panchenko EY, Kirillov VA, Timofeeva EE, Kretinina IV, Danil'son YN, Karaman I, Maier H, Cesari E. Russ Phys J+ 2012;54:937.

[64] Evirgen A, Basner F, Karaman I, Noebe RD, Pons J, Santamarta R. Funct Mater Lett 2012;5.

[65] Nishida M, Wayman CM, Chiba A. Metallography 1988;21:275.

[66] Hamilton RF, Sehitoglu H, Chumlyakov Y, Maier HJ. Acta Mater 2004;52:3383.

[67] Hornbogen E. Acta Metall Mater 1985;33:595.

[68] Voorhees PW. J Stat Phys 1985;38:231.

[69] Madras G, McCoy BJ. Chem Eng Sci 2004;59:2753.

[70] Madras G, McCoy BJ. J Chem Phys 2003;119:1683.

[71] Porter DA, Easterling KE. Phase transformations in metals and alloys. New York: Van Nostrand Reinhold, 1981.